Title
Identification of endogenous 1-aminopyrene as a novel mediator of progressive chronic kidney disease via aryl hydrocarbon receptor activation

Permalink
https://escholarship.org/uc/item/17v6k8j8

Journal
British Journal of Pharmacology, 177(15)

ISSN
0007-1188

Authors
Miao, Hua
Cao, Gang
Wu, Xia-Qing
et al.

Publication Date
2020-08-01

DOI
10.1111/bph.15062

Peer reviewed

RESEARCH PAPER

BJP | BRITISH PHARMACOLOGICAL SOCIETY

Identification of endogenous 1-aminopyrene as a novel mediator of progressive chronic kidney disease via aryl hydrocarbon receptor activation

Hua Miao[1] | Gang Cao[3] | Xia-Qing Wu[1] | Yuan-Yuan Chen[1] |
Dan-Qian Chen[1] | Lin Chen[1] | Nosratola D. Vaziri[2] | Ya-Long Feng[1] | Wei Su[4] |
Yi Gao[5] | Shougang Zhuang[6] | Xiao-Yong Yu[7] | Li Zhang[8] | Yan Guo[9] |
Ying-Yong Zhao[1]

[1]Faculty of Life Science & Medicine, Northwest University, Xi'an, Shaanxi, China

[2]Division of Nephrology and Hypertension, School of Medicine, University of California Irvine, Irvine, California, USA

[3]School of Pharmacy, Zhejiang Chinese Medical University, Hangzhou, Zhejiang, China

[4]Department of Nephrology, Baoji Central Hospital, Baoji, Shaanxi, China

[5]Department of Nephrology, The Affiliated Hospital of Northwest University, Xi'an, Shaanxi, China

[6]Department of Medicine, Rhode Island Hospital and Alpert Medical School, Brown University, Providence, Rhode Island, USA

[7]Department of Nephrology, Shaanxi Traditional Chinese Medicine Hospital, Xi'an, Shaanxi, China

[8]Department of Nephrology, Xi'an No. 4 Hospital, Xi'an, Shaanxi, China

[9]Department of Internal Medicine, University of New Mexico, Albuquerque, New Mexico, USA

Correspondence
Professor Ying-Yong Zhao, PhD, MD, Faculty of Life Science & Medicine, Northwest University, Xi'an, Shaanxi 710069, China.
Email: zyy@nwu.edu.cn

Background and Purpose: Increasing evidence has indicated that the high risk of cardiovascular disease in chronic kidney disease (CKD) patients cannot be sufficiently explained by classic risk factors.

Experimental Approach: Based on the least absolute shrinkage and selection operator method, we identified significantly altered renal tissue metabolites during progressive CKD in a 5/6 nephrectomized rat model and in CKD patients.

Key Results: Six aryl-containing metabolites (ACMs) were significantly increased from Week 1 to Week 20. They were associated with the activation of aryl hydrocarbon receptor (AhR) and its target genes including *CYP1A1*, *CYP1A2* and *CYP1B1*, which were further validated by molecular docking. Our study further demonstrated that AhR signalling could be activated by ACM in patients with idiopathic membranous nephropathy, diabetic nephropathy and IgA nephropathy. Most importantly, 1-aminopyrene (AP) showed strong positive and negative correlation with serum creatinine and creatinine clearance, respectively. AP significantly up-regulated the mRNA expressions of AhR and its three target genes in both mice and NRK-52E cells, while this effect was partially weakened in AhR small hairpin RNA-treated mice and NRK-52E cells. Furthermore, dietary flavonoid supplementation ameliorated CKD and renal fibrosis through partially inhibiting the AhR activity via lowering the ACM levels. The antagonistic effect of flavonoids on AhR was deeply influenced by the number and location of hydroxyl and glycosyl groups.

Conclusion and Implications: We uncovered that endogenous AP is a novel mediator of CKD progression via AhR activation; thus, AhR might serve as a promising target for CKD treatment.

---

1 | INTRODUCTION

Chronic kidney disease (CKD) is a major cause of high morbidity and mortality. The higher risk of cardiovascular disorders in chronic kidney disease patients cannot be sufficiently explained by classic factors such as tobacco use, high BP, obesity, diabetes mellitus and hypercholesterolaemia (Gansevoort et al., 2013). The uraemic environment itself is harmful and uraemic toxins play a critical role in chronic kidney disease patients. Uraemic toxins derived from tryptophan metabolism via the indolic pathway including indoxyl sulfate (IS) and indole-3-acetic acid (IAA) were recognized as endogenous aryl hydrocarbon receptor (AhR) ligands. Thus they could trigger aryl hydrocarbon receptor activation in patients with chronic kidney disease (Dou et al., 2015; Gondouin et al., 2013; Zhao et al., 2019). The aryl hydrocarbon receptor was initially discovered by virtue of its pivotal role as a mediator of toxic responses to environmental pollutants and chemicals, including halogenated aromatic hydrocarbons and polycyclic aromatic hydrocarbons (PAHs), such as 2,3,7,8-tetrachlorodibenzo-p-dioxin (Iu et al., 2017; Shinde & McGaha, 2018). Recently, studies have shown that aryl hydrocarbon receptor can be activated not only by a myriad of xenobiotics from the environment, diet and microbiome but also by several endogenous ligands involved in the regulation of organ development and tissue homeostasis under normal and disease states (Dolivo, Larson, & Dominko, 2018; Gutierrez-Vazquez & Quintana, 2018; Lamas et al., 2016). Mounting evidence has demonstrated that the activation of aryl hydrocarbon receptor is associated with an increased risk of cancer, chronic kidney disease and autoimmune disorders (Cheong & Sun, 2018; Corre et al., 2018; Song, Ramprasath, Wang, & Zou, 2017).

Extensive studies have suggested that tryptophan-derived indoxyl sulfate and indole-3-acetic acid are endogenous aryl hydrocarbon receptor ligands that trigger aryl hydrocarbon receptor activation (Brito et al., 2017; Sallee et al., 2014). A study reported that indole metabolites up-regulated tissue factor expression by an aryl hydrocarbon receptor-dependent pathway during Stages 3–5D in chronic kidney disease patients. Up-regulated tissue factor expression was positively correlated with the levels of serum indoxyl sulfate and indole-3-acetic acid in patients with chronic kidney disease (Gondouin et al., 2013). Indoxyl sulfate and indole-3-acetic acid further up-regulated the expression of eight aryl hydrocarbon receptor downstream genes including CYP1A1, CYP1A2 and CYP1B1 in human umbilical vein endothelial cells (Gondouin et al., 2013). Another study revealed that indole-3-acetic acid activated the aryl hydrocarbon receptor/NF-κB pathway, which mediated COX-2 expression and indole-3-acetic acid elevated the production of ROS both in vivo and in vitro (Dou et al., 2015). In addition, the indoxyl sulfate level significantly correlated with aryl hydrocarbon receptor activity in patients with

What is already known

- AhR is a cytoplasmic transcription factor receptor activated in CKD which mediates renal fibrosis.
- Tryptophan-derived metabolites including indoxyl sulfate and indole-3-acetic acid were recognized as endogenous AhR ligands.

What this study adds

- 1-Aminopyrene activated AhR and target genes mediates renal fibrosis in both mice and NRK-52E cells.
- Flavonoid supplementation ameliorated CKD and renal fibrosis by inhibiting AhR signalling via lowering ACM.

What is the clinical significance

- AhR may be a promising therapeutic target strategy for treating CKD and renal fibrosis.

end-stage renal disease (ESRD) (Shivanna et al., 2016). The least absolute shrinkage and selection operator is a regularized regression technique well suited for reduction of high-dimensional data to select differential metabolites (Chung et al., 2019; Li et al., 2018). Using the 5/6 nephrectomized (NX) chronic kidney disease rat model, we first developed a logistic least absolute shrinkage and selection operator-based feature selection model on the m/z data set to select the strongest metabolite determinants of chronic kidney disease progression by ultra-performance LC (UPLC) coupled with high-definition mass spectrometry-based metabolomics. Secondly, we investigated whether aryl hydrocarbon receptor expression could be activated by identifying endogenous aryl-containing metabolites (ACMs) as ligands in 5/6 nephrectomized rats and in patients with idiopathic membranous nephropathy (IMN), diabetic nephropathy (DN) and IgA nephropathy (IgAN). Thirdly, we identified three new aryl hydrocarbon receptor antagonists, 5,7,3′,4′,5′-pentahydroxy flavanone (PHF), barleriside A (BSA) and rhoifolin (RHO), which were isolated from Semen Plantaginis. These compounds retarded renal fibrosis by suppressing aryl hydrocarbon receptor and its target gene expression, through mediation by aryl-containing metabolite, in chronic kidney disease rats.

2 | METHODS

2.1 | Patient selection

Serum and urine were collected from 52 patients with idiopathic membranous nephropathy, 50 patients with diabetic nephropathy and 51 patients with IgA nephropathy, as well as 50 age-matched healthy controls who underwent renal biopsy or donors between February 2011 and November 2018 at Shaanxi Traditional Chinese Medicine Hospital, Xi'an No. 4 Hospital, Xi'an Jiaotong University and Baoji Central Hospital. All patients provided informed consent to participate in the study. All participants were ethnic Chinese and the estimated GFR (eGFR) was calculated by the modified chronic kidney disease Epidemiology Collaboration equation since it could improve the accuracy of GFR determination in Chinese chronic kidney disease patients (Wang et al., 2016). Patients with cancer, active vasculitis, liver disease, gastrointestinal pathology or acute kidney injury were excluded from the study. Healthy controls were excluded if they had any of the following conditions:- diabetes, hypertension, cardiovascular disease, kidney dysfunction or use of regular medications. Serum samples were obtained after an overnight fasting and the blood biochemistry was determined by the clinical laboratory. The sample collection was approved by the Shaanxi Traditional Chinese Medicine Hospital (Permit Number SXSY-235610). The study was approved by the Ethical Committee of Northwest University and all procedures were conducted in accordance with the Helsinki Declaration.

2.2 | Animal experimental design

All animal care and experimental procedures were approved by the Ethics Committee for Animal Experiments of Northwest University (No. SYXK2010-004). Eight-week-old male Sprague–Dawley rats (6–8 weeks old, weighing 190–210 g, RRID:RGD_728193) and male C57BL/6 mice (6–8 weeks old, weighing 20–25 g) were purchased from the Central Animal Breeding House of Xi'an Jiaotong University (Xi'an, Shaanxi, China). The mice were provided food and water ad libitum and housed in plastic cages (≤5 mice per cage) placed in a specific pathogen-free air-conditioned vivarium under 40%–70% humidity at 22 ± 2°C and a 12-h light/12-h dark cycle. They were acclimatized to their housing environment for 7 days prior to experimentation and to the experimental room for 1 h before the experiments. Animal studies are reported in compliance with the ARRIVE guidelines (Kilkenny, Browne, Cuthill, Emerson, & Altman, 2010) and with the recommendations made by the *British Journal of Pharmacology*.

The rats were randomly divided into two groups, sham and 5/6 nephrectomized groups. Briefly, following anaesthesia with sodium pentobarbital by intraperitoneal injection (3%, 10 ml·kg^{-1}), 2/3 portion of the left kidney was excised. Subsequently, the whole right kidney was removed by scalpel excision after 1 week. Gelfoam coagulant was further applied on the cut surfaces, while the sham group was treated under the same surgical procedure without nephrectomy operation. Eight 5/6 nephrectomized rats were selected randomly, anaesthetized with 10% urethane and killed at Weeks 0, 1, 2, 3, 4, 5, 6, 9, 12 and 20. The remnant kidneys were collected for the following studies.

To study the effect of 1-aminopyrene (AP) on aryl hydrocarbon receptor expression, C57BL/6 mice were randomized into two groups (n = 24), control and 1-aminopyrene-treated groups. The AP-treated group was given 200 mg·kg^{-1} 1-aminopyrene through oral gavage every day, whereas the control mice received the same volume of normal saline. Six mice were selected from each of the two groups, randomly anaesthetized with 10% urethane and killed at Weeks 0, 3, 6 and 9. The kidneys were collected for the following studies.

In order to examine the potential of barleriside A and 5,7,3′,4′,5′-pentahydroxy flavanone as novel aryl hydrocarbon receptor antagonists, the rats were randomized into the sham, 5/6 nephrectomized, 5/6 nephrectomized + barleriside A and 5/6 nephrectomized + 5,7,3′,4′,5′-pentahydroxy flavanone groups (n = 8). Once daily, from the ninth to 12th week, 10 mg·kg^{-1} barleriside A and 5,7,3′,4′,5′-pentahydroxy flavanone were administered to the 5/6 nephrectomized + barleriside A and 5/6 nephrectomized + 5,7,3′,4′,5′-pentahydroxy flavanone groups, respectively, by oral gavage and all rats were killed at the 12th week. For biochemical analysis, 24-h urine and serum samples were collected, while the remnant kidney in the 5/6 nephrectomized rats was collected for the following studies.

2.3 | Metabolomic analysis

The kidney tissue samples from rats and humans were analysed using a 2.1 mm × 100 mm ACQUITY 1.8-μm HSS T3 column on a Waters Acquity™ UPLC system equipped with a Waters Xevo™ G2 QTof MS (Milford, MA, USA). Metabolomic procedures including sample preparation, metabolite separation and detection, data pre-processing and statistical analysis for metabolite identification were performed following our previous protocols with minor modifications (Chen, Cao, et al., 2019; Feng et al., 2019; Zhao, Cheng, et al., 2013; Zhao, Liu, Cheng, Bai, & Lin, 2012).

2.4 | Knockdown of aryl hydrocarbon receptor in mice and knockdown and knockin of aryl hydrocarbon receptor in NRK-52E cells

Adenovirus carrying small hairpin RNA (shRNA) against aryl hydrocarbon receptor or non-specific shRNA (scramble) was designed and constructed by Sangon (Shanghai, China). The lentivirus delivery was performed as previously described with minor modifications (Hao, Bellner, & Ferreri, 2013; Kim et al., 2009). After anaesthesia, the fur of the mice was shaved off. The left kidney of the mouse was exposed surgically. During the injection, the renal vein, artery and ureter were avoided. The depth of the needle was approximately 0.5 cm and

100 μl of virus was injected in 2–3 s. The mice were injected with recombinant lentivirus vector by a 31-G needle at the lower pole of the kidney parallel to the long axis. Next, 100 μl of lentivirus cocktail (1×105 IU·μl^{-1}) were injected into the kidney. After the injection, the needle was removed after waiting for 2–3 s. The kidney was carefully replaced and the wound was sutured. The kidney tissues were collected at Week 9 after the injection and the effect of the shRNA against aryl hydrocarbon receptor was determined by aryl hydrocarbon receptor mRNA expression.

Normal rat kidney proximal tubular epithelial cells NRK-52E (JCRB Cat# IFO50480, RRID:CVCL_0468) were transfected with 3 μl of 10-μM shRNA aryl hydrocarbon receptor or scramble per well, as per by using Lipofectamine RNAiMAX (Invitrogen, New York, USA). NRK-52E cells were also transfected with lentivirus expressing full-length aryl hydrocarbon receptor cDNA (aryl hydrocarbon receptor over) or vector according to the manufacturer's protocols. Cell samples were processed by quantitative RT-PCR (qRT-PCR) and Western blot analysis.

2.5 | Cell viability analysis

NRK-52E cells were cultured in DMEM-F12 supplemented with 10% FBS at 37°C with 5% CO_2 and a CCK-8 kit was used to detect cell viability based on the manufacturer's protocol. Next, 1×10^4 cells plated in 96-well plates were treated with 0, 2.5, 5, 10, 20 and 40 nM of 1-aminopyrene (98% purity, Sigma-Aldrich, St. Louis, MO, USA) for 24 h or 10 nM of 1-aminopyrene for 0, 6, 12, 24, 48 and 72 h, while cells treated with 0.1% DMSO were employed as the vehicle control. The absorbance of each pore at 450 nm was detected using a microplate reader. Moreover, the cell viability at each concentration was measured repeatedly for six times.

2.6 | 1-Aminopyrene-mediated effect on aryl hydrocarbon receptor and antagonistic effect of flavonoids in NRK-52E cells

In order to analyse the effect of 1-aminopyrene on the expressions of the aryl hydrocarbon receptor mRNA and protein, the NRK-52E cells were exposed to 1-aminopyrene (0, 0.1, 1 and 10 nM) for 24 h or 10 nM of 1-aminopyrene for 0, 6, 12 and 24 h. Additionally, the NRK-52E cells were co-cultured with 1-aminopyrene (10 nM) and 10 μM of 5,7,3′,4′,5′-pentahydroxy flavanone, barleriside A or rhoifolin for 24 h to investigate the antagonistic effect of flavonoids on 1-aminopyrene-induced aryl hydrocarbon receptor expression. CH223191 (10 μM) was used as the positive control.

2.7 | Luciferase assay

Aryl hydrocarbon receptor activity was determined in the NRK-52E cells using a luciferase reporter assay system kit (Promega, Madison,

WI, USA) (Ma et al., 2019; Zhang et al., 2018). NRK-52E cells were treated with 1-aminopyrene with or without an aryl hydrocarbon receptor antagonist for 24 h. Cell luciferase activity was detected by using a luciferase detection system substrate based on the manufacturer's directions.

2.8 | Renal function evaluation and BP

Serum creatinine, urine creatinine and proteinuria were measured using an Olympus AU6402 automatic analyser. The urine protein/creatinine ratio and creatinine clearance rate (Ccr) were calculated. Systolic BP (SBP) was measured weekly through the rat tail-cuff BP instrument (Techman Soft, Chengdu, Sichuan, China) and all rats were acclimatized to this procedure for 1 week before measurement. The measurement of SBP was carried out between 8:00 and 11:00 am to avoid the influence of the circadian rhythm on BP and heart rate. Six measurements were obtained in each rat at 2- to 3-min intervals and the mean values of SBP were calculated.

2.9 | Light microscopic study

A light microscopic study was performed on 10% formalin-fixed, paraffin-embedded biopsies that were stained with haematoxylin–eosin (HE), Periodic Acid-Schiff (PAS) and Masson's trichrome staining, as previously described (Zhang et al., 2016; Zhang et al., 2015). The sections (5 μm) were stained using the Periodic Acid-Schiff method and used for histological analyses. The total number of glomeruli on each slide was counted and assessed for each rat (range 30 to 120). The incidence of glomerular sclerosis, tubular dilation/hyaline deposition and interstitial fibrosis was quantitatively assessed, as previously described (Lin et al., 2002). The extent of glomerular damage was assessed by examining 50 glomeruli in each rat and calculated as the percentage of glomeruli presenting focal or global sclerotic lesions (Iyoda, Shibata, Hirai, Kuno, & Akizawa, 2011). Glomerulosclerosis was evaluated using a semiquantitative score from 0 to 4 (0, no sclerosis; 1, sclerosis up to 25% of glomeruli; 2, sclerosis from 25% to 50% of glomeruli; 3, zsclerosis from 50% to 75% of glomeruli and 4, sclerosis >75% of glomeruli) and the glomerulosclerosis score was obtained as follows:- [(1 × number of glomeruli with +1) + (2 × number of glomeruli with +2) + (3 × number of glomeruli with +3) + (4 × number of glomeruli with +4)] × 100/ total number of glomeruli examined (Iyoda et al., 2011). Tubulointerstitial damage was defined as inflammatory cell infiltrates, tubular dilation and/or atrophy or interstitial fibrosis. Tubulointerstitial damage was examined in successive fields in entire cortical and juxtamedullary areas that were suitable for specimen evaluation by computer-assisted image analysis; the damage was scored on a 0 to 5 scale (Grade 0, no changes; Grade 1, <10%; Grade 2, 10% to 25%; Grade 3, 25% to 50%; Grade 4, 50% to 75% and Grade 5, 75% to 100%), as described in our previous study

(Rodriguez-Iturbe et al., 2005), depending on the extent of interstitial infiltration, tubular dilatation and fibrosis (Rodriguez-Iturbe et al., 2005). All histological analyses were performed by two investigators in a blinded manner.

2.10 | Immunohistochemistry

The Immuno-related procedures used comply with the recommendations made by the *British Journal of Pharmacology* (Alexander et al., 2018). aryl hydrocarbon receptor, collagen I and α-smooth muscle actin (α-SMA) expression was evaluated using paraffin sections of kidney tissues. After antigen retrieval in citrate buffer or fixation in acetone for 10 min, the sections were treated with H_2O_2 to eliminate endogenous peroxidase activity and blocked with avidin–biotin and biotin–streptavidin. The sections were then incubated overnight at 4°C with primary antibodies against anti-aryl hydrocarbon receptor (ab84833), anti-collagen I (ab34710) and anti-α-SMA (ab7817). Next, the sections were washed with PBS and treated with a goat anti-rabbit (PV-6001, ZSGB-BIO, Beijing, China) or goat anti-mouse (PV-6002, ZSGB-BIO) secondary antibody for 1 h. Diaminobenzidine was used as a chromogen. Results are expressed as the percentage of positively stained area. Evaluations were performed by two investigators in a blinded fashion. Image analysis was performed by using the Image-Pro Plus (Media Cybernetics, Bethesda, MD, RRID: SCR_007369).

2.11 | Immunofluorescence

HK-2 cells were cultured on coverslips and fixed with 4% paraformaldehyde for 10 min at 4°C. After being blocked with normal goat serum for 30 min, the cells were incubated with primary antibody directly against anti-aryl hydrocarbon receptor (ab84833) at 4°C overnight. The secondary antibodies Alexa Fluor® 488 conjugated goat anti-rabbit IgG H&L were incubated for 2 h at room temperature. DAPI was used to detect nuclear localization. The stained cells were mounted with 80% glycerol/PBS for subsequent examination using a laser-scanning confocal microscope (FV1000, Olympus, Japan) with FV10-ASW 4.0 VIEW.

2.12 | Quantitative real-time PCR

Total RNA was extracted and isolated from the renal cortex or cells by Trizol reagent (RNAiso Plus, Takara Bio, Japan) according to the manufacturer's instructions. The qRT-PCR analysis was performed as we previously described (Wang et al., 2018). The primers were synthesized by Sangon Biotech (Shanghai, China); the specific primers are listed in Table S1. The gene expressions were normalized by the housekeeping gene β-actin and the fold increase over the control values was calculated by relative quantification using the $2^{-\Delta\Delta Ct}$ method.

2.13 | Western blot analysis

All solutions, tubes and centrifuges were maintained at 0°C to 4°C. Cytoplasmic and nuclear extracts were prepared according to our previous study (Choi, Lim, & Hong, 2010). Briefly, after harvesting cells with trypsin–EDTA and washing them with PBS, the cells were moved to a 1.5-ml microcentrifuge tube and centrifugated at 500×g for 3 min and the supernatant was discarded. The kidney tissue was cut into small pieces in a microcentrifuge tube and centrifugated at 500×g for 5 min and the supernatant was discarded. Next, ice-cold cytoplasmic extraction reagent I was added to the cell pellet or homogenized tissue. After vortexing the tube vigorously for 15 s, it was incubated on ice for 10 min. Ice-cold cytoplasmic extraction reagent II was added to the tube. After vortexing the tube for 5 s, it was incubated for 1 min on ice. The tube was centrifuged for 5 min at maximum speed in a microcentrifuge. The supernatant was the cytoplasmic extract and it was transferred to a clean pre-chilled tube. The insoluble fraction was suspended in ice-cold nuclear extraction reagent and after vortexing for 15 s, the tube was vortexed every 10 min at maximum speed for a total of 40 min. The tube was centrifuged at maximum speed for 10 min. The supernatant was the nuclear extract and it was transferred to a clean pre-chilled tube. The supernatant containing nuclear proteins was stored at −80°C. The protein concentrations in the tissue homogenates and nuclear extracts were determined by the Bio-Rad protein assay. Western blot analysis was carried out as previously described (Wang et al., 2018; Zhang et al., 2016). The primary antibodies including anti-aryl hydrocarbon receptor, anti-collagen I, anti-α-smooth muscle actin, anti-fibronectin, anti-vimentin, anti-fibroblast-specific protein 1 (FSP1) and anti-E-cadherin were purchased from Abcam Company (Cambridge, MA, USA) or Santa Cruz Biotechnology (Santa Cruz, CA, USA). Secondary antibodies including goat anti-rabbit or goat anti-mouse were purchased from Abbkine Scientific Co., Ltd (CA, USA). Briefly, the lysates were separated by 10% SDS-PAGE and electrophoretically transferred onto PVDF membranes (Millipore Corp., Bedford, MA, USA). The membranes were incubated in 1× Tris-buffered solution, 0.1% Tween-20 and 5% non-fat milk blocking buffer for 1 h at room temperature, probed with the indicated primary antibodies overnight at 4°C and then incubated with a goat anti-rabbit (A21020) or goat anti-mouse (Abbkine Cat# A21010, RRID: AB_2728771) secondary antibody. The blots were developed using enhanced chemiluminescence reagent and the protein levels were normalized to GAPDH or α-tubulin expression. Specific bands indicating target proteins were analysed using the ImageJ 1.48v software (RRID:SCR_003070).

2.14 | Molecular ligand docking and binding energy calculations

The chemical structures of six aryl-containing metabolites and three flavonoids were sketched on the ACD/ChemSketch tool and energy minimization of both the target aryl hydrocarbon receptor and the compounds was optimized on Molecular Operating Environment

(MOE 2014.0901). The Periodic Acid-Schiff domain of the aryl hydrocarbon receptor is the ligand-binding domain. The structures of several period [Per]-aryl hydrocarbon receptor nuclear translocator [Arnt]-single minded [Sim] (Periodic Acid-Schiff) domains are currently available in the protein data bank (Protein Data Bank id: 4ZPR, identities: 32%), which are selected for establishing a homology model of the mouse aryl hydrocarbon receptor-ligand-binding domain according to their structure similarity with aryl hydrocarbon receptor in this region (Bisson et al., 2009). Docking analyses were carried out using the program AutoDock 4.0 (RRID:SCR_012746) to predict the conformation and orientation of the ligand on the surface of the Periodic Acid-Schiff-B domain of aryl hydrocarbon receptor. Each of the aryl hydrocarbon receptor ligand-binding domains was generated by using the homology model protocol as previously described (Ginalski, 2006). The mouse aryl hydrocarbon receptor- ligand-binding domain homology model was used to characterize the ligand-binding pocket when the model was established. Additionally, this aryl hydrocarbon receptor- ligand-binding domain homology model was used to structurally analyse metabolites with high binding affinity towards aryl hydrocarbon receptor. The lower equilibrium dissociation constant (K_D) was calculated.

2.15 | Desorption electrospray ionization mass spectrometry imaging

Flash-frozen kidney tissue slides were thawed at room temperature before being analysed by desorption electrospray ionization mass spectrometry. Desorption electrospray ionization mass spectrometry imaging for the distribution of 1-aminopyrene in the kidney tissues of the mice was carried out on a Xevo G2-XS Q-TOF mass spectrometer (Waters Corporation, Milford, MA) equipped with a two-dimensional DESI source (Waters Corporation) and a custom-built inlet capillary heated to 490°C. DESI parameters were optimized for the best spatial resolution and signal intensity on the kidney tissues and were as follows: solvent, methanol/water, 95:5; flow rate, 0.5 μl·min^{-1}; nebulizing gas, nitrogen; gas pressure, 4.5 bar; sprayer incidence angle, 75°; spray voltage, 4.5 kV; cone voltage, 80 V; collection angle, 10°; sprayer-to-inlet distance, 10 mm; sprayer-to-sample distance, 1.5 mm; 0.1-mM NH_4Cl and 0.1-mM leucine enkephalin delivered at 1.5 μl·min^{-1}; mass range, m/z, 100–1,200; and X and Y pixel size, 50 μm. Mass spectrometric parameters were as follows: source offset, −80 V; source temperature, 120°C; and scan time, 4 s. The spectra were recalibrated for high mass accuracy by using the accurate mass of leucine enkephalin as the lock mass (m/z 554.2615) present in the solvent spray. The desorption electrospray ionization-mass spectrometry imaging was performed for 1-aminopyrene (m/z 218.09, +H adduct) in the positive ion mode. The mass spectrometry imaging data for the kidney tissues were obtained from raw mass spectrometry files by using the High Definition Imaging package (Waters Corporation) and MassLynx version 4.1 (Waters, Milford, MA, USA, RRID: SCR_014271).

2.16 | Statistics analysis

The data and statistical analysis comply with the recommendations of the *British Journal of Pharmacology* on experimental design and analysis in pharmacology (Curtis et al., 2018). The number of replicates was six to eight per group for each data set and the results were presented as the mean ± SEM unless stated otherwise. Statistical analyses were performed with R 2.15.0 and the GraphPad Prism software v 6.0 (San Diego, CA, USA, RRID:SCR_002798). A two-tailed unpaired Student's *t* test was used for the comparison between two groups and statistically significant differences among more than two groups were analysed using one-way ANOVA followed by Dunnett's post hoc tests when *F* achieved $P < 0.05$ and there was no significant variance in homogeneity. Some results were normalized to the control to avoid unwanted sources of variation. $P < 0.05$ was considered to indicate significant differences. Principal component analysis (PCA) was performed using the MarkerLynx XS software (Waters Corporation) to cluster the sample plots across different groups.

2.17 | Materials

All materials were purchased from Sigma-Aldrich unless otherwise stated. Details of the primer sequences used in the study are shown in Supporting Information.

2.18 | Nomenclature of targets and ligands

Key protein targets and ligands in this article are hyperlinked to corresponding entries in http://www.guidetopharmacology.org, the common portal for data from the IUPHAR/BPS Guide to PHARMACOLOGY (Harding et al., 2018) and are permanently archived in the Concise Guide to PHARMACOLOGY 2019/20 (Alexander, Fabbro, et al., 2019; Alexander, Kelly, et al., 2019).

3 | RESULTS

3.1 | Renal function and histology

As shown in Figure 1a, following 5/6 nephrectomized, the rats exhibited significantly elevated SBP and serum creatinine levels. 5/6 nephrectomized led to significant proteinuria accompanied by a significant decrease in creatinine clearance rate and gradual loss of renal function that caused progressive renal damage, leading to end-stage renal disease. Morphologically, slight kidney damage was observed at the early stages of 5/6 nephrectomized. 5/6 nephrectomized resulted in typical tubulointerstitial fibrosis (TIF) at week 9; 5/6 nephrectomized exhibited focal segmental glomerulosclerosis and glomerulosclerosis at Weeks 12 and 20, respectively (Figure 1b). Initially, progressive renal injury only existed in localized areas of the renal cortex, while hypertrophy, TIF and glomerulosclerosis spread
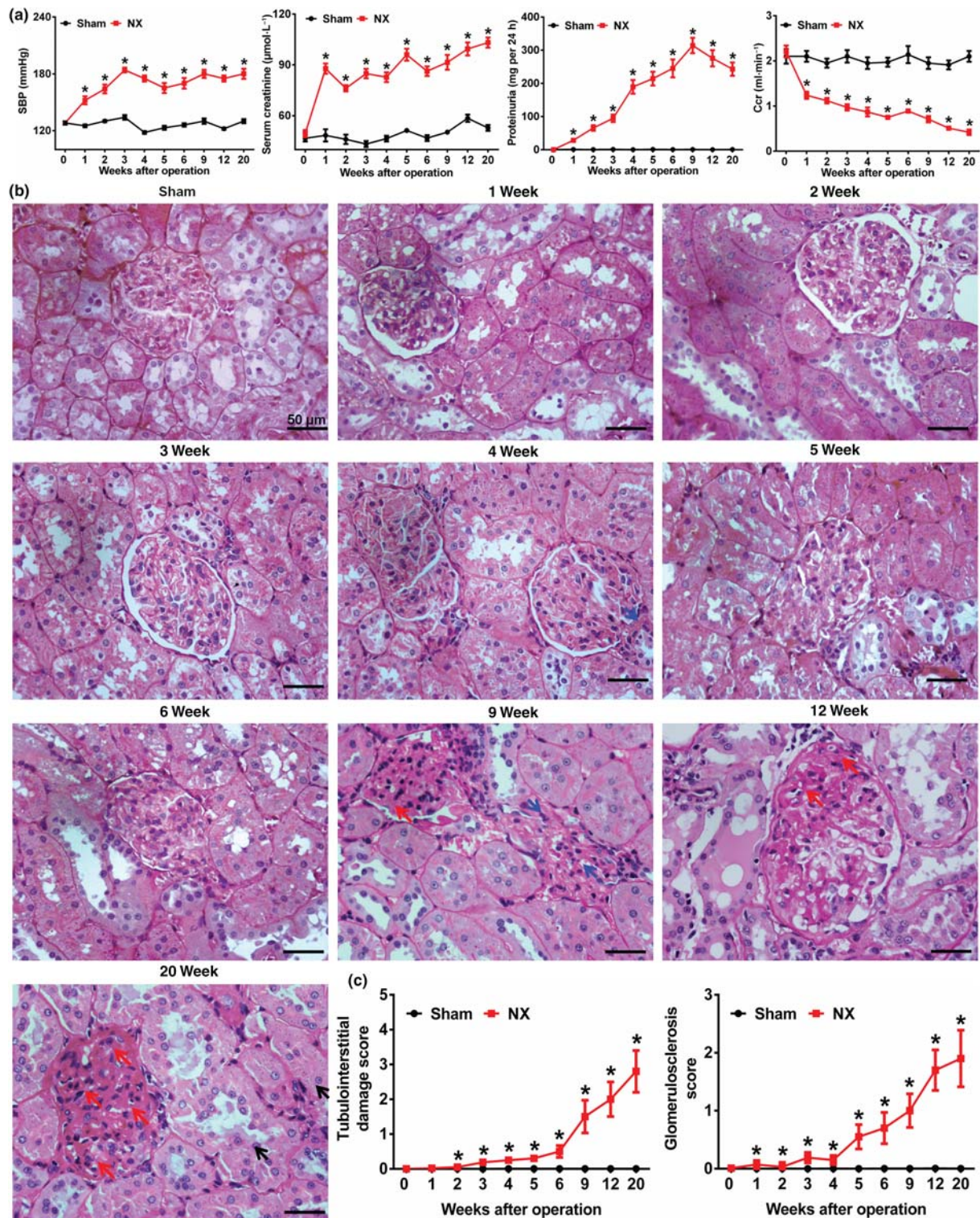
FIGURE 1   Analysis of BP, kidney function and renal damage after 5/6 nephrectomized (NX) in rats. (a) Biochemical indexes including systolic BP, serum creatinine, 24-h urinary protein excretion and GFR measured by creatinine clearance rate (Ccr). (b) Light microscopic results in the study groups. Representative pictures stained with Periodic Acid-Schiff (PAS). (c) Morphologic evaluation of the scores of tubulointerstitial fibrosis and glomerulosclerosis in the study groups. Blue arrows indicate tubulointerstitial fibrosis at Week 9; red arrows indicate focal segmental glomerulosclerosis at 12 weeks and glomerulosclerosis at 20 weeks. $^{*}P < 0.05$ versus sham-operated group

widely throughout the cortex area as the disease progressed from Weeks 9 to 20 (Figure 1c).

3.2 | Significantly altered metabolic profile in the course of chronic kidney disease progression

To evaluate the systemic changes in the metabolome of the rat remnant kidney tissue, untargeted metabolomics was performed in both positive and negative ion modes. A two-predictive component principal component analysis was performed by using all the metabolite ions from the sham and 5/6 nephrectomized rats at Weeks 0, 1, 2, 3, 4, 5, 6, 9, 12 and 20. As shown in Figure 2a, unsupervised principal component analysis score plots showed the significantly altered metabolic profile between the healthy rats and the rats at different stages of chronic kidney disease. Furthermore, principal component analysis can be used to distinguish the different stages of progressive chronic kidney disease, indicating that the tissue metabolic pattern was significantly altered in the remnant kidney (Figure 2a). The metabolic trajectories in the 5/6 nephrectomized rats (first week) shifted away from that in the sham rats along the $t[1]$ axis, with a maximum shift reached by the 20th week (Figure 2a). Intriguingly, the principal component analysis showed that the 5/6 nephrectomized rats at Week 3 were completely separated from the 5/6 nephrectomized rats at Weeks 1 and 2, as well as from the 5/6 nephrectomized rats at Weeks 4, 5 and 6. The 5/6 nephrectomized rats at Week 1 were not completely separated from those at Week 2. Similarly, there was partial separation among 5/6 nephrectomized rats at Weeks 4, 5 and 6. Furthermore, 5/6 nephrectomized might lead to the development of early renal injury before the third week, which further shifts to progressive chronic kidney disease and finally progresses to end-stage renal disease, suggesting that 5/6 nephrectomized rats at Week 3 may be at a critical phase in the progression of chronic kidney disease. Therefore, the 5/6 nephrectomized rats at Week 2 were recognized as being in the early stages of chronic kidney disease, while the 5/6 nephrectomized rats at Week 2 shifted to progressive chronic kidney disease, which led to end-stage renal disease. In addition, the 5/6 nephrectomized rats at Week 9 represented typical chronic kidney disease. In summary, these findings indicated that 5/6 nephrectomized led to a significant alteration in metabolites in progressive chronic kidney disease, which was highly consistent with a previous study (Dolkart, Khoury, Amar, & Weinbroum, 2014).

3.3 | Significantly increasing aryl-containing metabolite during progressive chronic kidney disease

A list of exact m/z values with the highest statistical significance was selected via least absolute shrinkage and selection operator, representing the important metabolite features based on the complete data. We analysed and compared the renal injury process from sham to chronic kidney disease at Week 20 by calculating the changes in

the trend of P value using the least absolute shrinkage and selection operator method. Based on the change in trend, $P < 0.05$, a total of 3,048 m/z variables were selected and identified from positive and negative ion modes (Zhao, Cheng, Cui, et al., 2012; Zhao, Cheng, Wei, et al., 2012; Zhao, Zhang, et al., 2013). After excluding xenobiotics and different fragment ions from the same metabolites, 216 metabolites were identified (Tables 1, S2, S3, S4 and S5), which were mainly classified into two categories: 57 aryl-containing metabolites, namely, four polycyclic aromatic hydrocarbons, seven indoles and 46 compounds with one benzene ring and 159 other compounds with different numbers of benzene rings.

Intriguingly, two polycyclic aromatic hydrocarbon metabolites (1-aminopyrene and 1-hydroxypyrene), two indole metabolites (IS; indole-3-acetic-acid-O-glucuronide and 14 metabolites with one benzene ring were significantly increased throughout the entire study period in the 5/6 nephrectomized rats compared to that in the sham rats (Table 1), indicating that these aromatic hydrocarbons might have an important effect on chronic kidney disease progression. Seventeen other type metabolites were significantly increased throughout the study period in the 5/6 nephrectomized rats compared to that in the sham group as well, while two other type metabolites were significantly decreased (Table S2). After 3 weeks, 108 metabolites were significantly increased in the 5/6 nephrectomized rats (Table S4), which may be biomarkers of progressive chronic kidney disease or end-stage renal disease. Moreover, two other polycyclic aromatic hydrocarbons including 1-methoxypyrene and atherospermidine were significantly increased after 5 weeks in the 5/6 nephrectomized rats (Table 1), which may be potential biomarkers for progressive chronic kidney disease or end-stage renal disease. Furthermore, 27 metabolites were significantly increased at certain time points in the 5/6 nephrectomized rats compared to that in the sham group (Table S3). In addition, trend P values of 42 metabolites were only less than 0.05 (Table S5). Therefore, we speculated that significantly increased aryl-containing metabolite might activate aryl hydrocarbon receptor in 5/6 nephrectomized rats. Heatmap analysis was performed by using 20 aryl-containing metabolites that were significantly increased (Figure 2b) and it demonstrated that the aryl-containing metabolite gradually increased from the sham rats to 20-week 5/6 nephrectomized rats, which indicated progressive chronic kidney disease (Figure 2b). Interestingly, six aryl-containing metabolites displayed a significantly increasing trend from the sham rats to 20-week 5/6 nephrectomized rats (Figure 2c), three of which were typical polycyclic aromatic hydrocarbon (Figure 2d). Among these three metabolites, 1-aminopyrene, 1-hydroxypyrene and 1-methoxypyrene were positively correlated with the serum creatinine level and negatively correlated with creatinine clearance rate, while 1-aminopyrene exhibited the highest significance (Figure 2e). To further verify whether aryl hydrocarbon receptor signalling was activated by aryl-containing metabolite in patients, 203 patients and healthy controls were used for studying the relationship among the expressions of six aryl-containing metabolites and aryl hydrocarbon receptor. Baseline characteristics of the healthy

controls and patients are shown in Table S6. Compared to healthy controls, six aryl-containing metabolites were significantly increased in patients with idiopathic membranous nephropathy, diabetic nephropathy and IgA nephropathy (Figure 2f). In summary, chronic kidney disease progression paralleled significantly with increased aryl-containing metabolite.

3.4 | Aryl hydrocarbon receptor activation and its downstream gene expression during chronic kidney disease progression

To investigate whether 5/6 nephrectomized directly activates aryl hydrocarbon receptor signalling in the remnant kidney, the mRNA
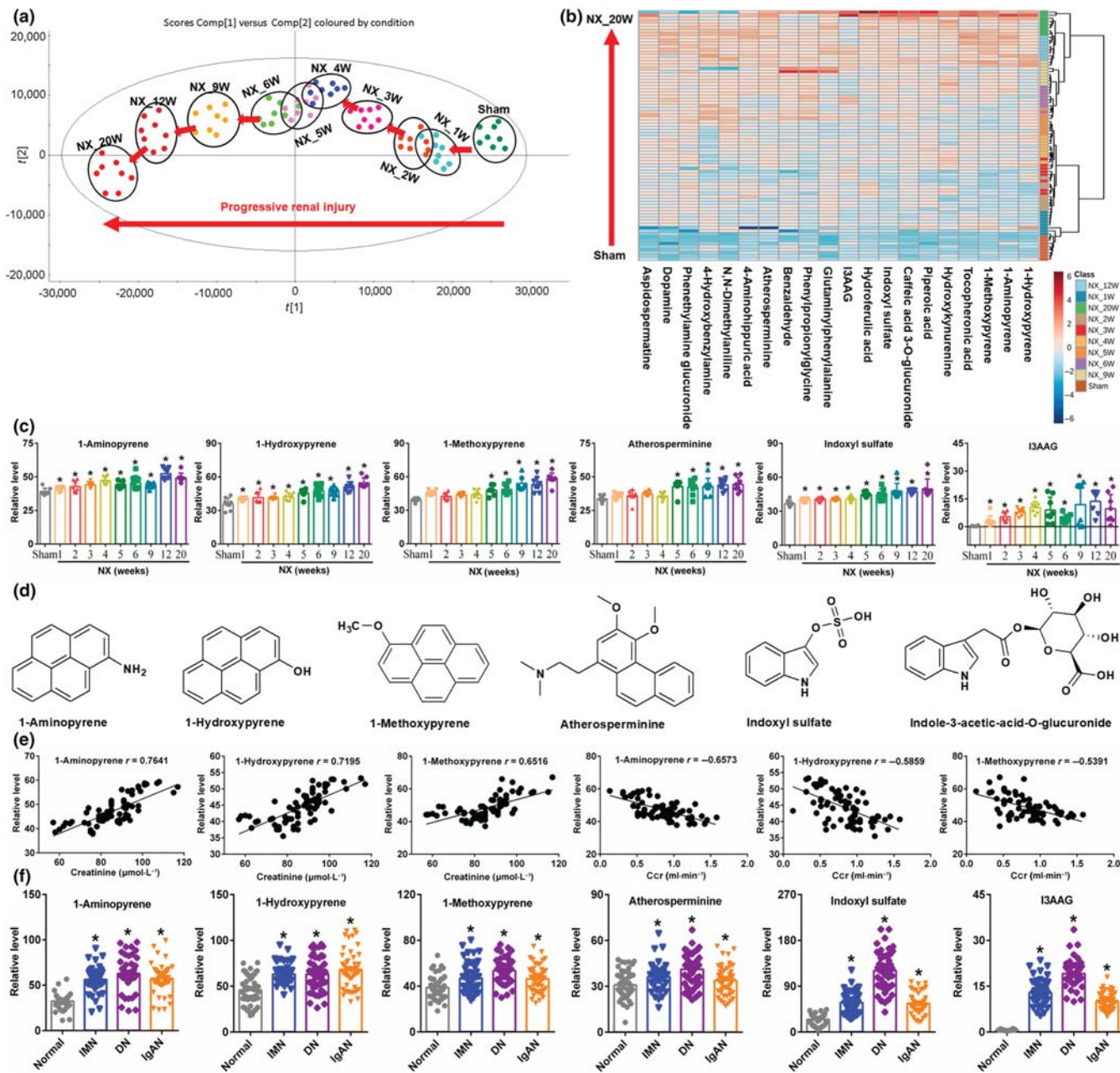

FIGURE 2 Progressive chronic kidney disease (CKD) was accompanied by significantly increased aryl-containing metabolite (ACM) levels. (a) Visualization of changes in the metabolic trajectories in 5/6 nephrectomized (NX) rats. Principal component analysis (PCA) score plot of metabolic profiles throughout the entire study period in positive ion mode. (b) Heatmap of 20 aryl-containing metabolites throughout the entire study period. The colour of each section is proportional to the significance of change in metabolites (red, increased; blue, decreased). Rows: samples; columns: metabolites. (c) The relative levels of the six significantly increased aryl-containing metabolites throughout the entire study period. The dot represents a single-data point in the bar graph. *$P < 0.05$ versus sham group ($n = 8$). (d) The chemical structure of the six ACMs, as indicated. (e) The associations between three polycyclic aromatic hydrocarbons (PAHs) and serum creatinine or creatinine clearance rate (Ccr) throughout the entire study period. (f) The relative levels of the six significantly increased ACMs in patients with idiopathic membranous nephropathy (IMN), diabetic nephropathy (DN) and IgA nephropathy (IgAN). *$P < 0.05$ versus normal group

TABLE 1 Significantly differential kidney tissue metabolites, *P* value and compound types between sham group and different time points of 5/6 nephrectomized (NX) groups

Metabolites	1W_P^a	2W_P^a	3W_P^a	4W_P^a	5W_P^a	6W_P^a	9W_P^a	12W_P^a	20W_P^a	Trend_P^b	Trend[c]	Types
1-Aminopyrene	3.51E-02	4.75E-02	6.22E-04	3.10E-05	1.36E-03	6.97E-03	2.84E-02	1.64E-06	7.67E-06	1.30E-05	1	PAH
1-Hydroxypyrene	3.08E-02	4.47E-02	2.05E-02	1.36E-02	8.75E-04	5.85E-04	3.58E-04	2.42E-05	2.29E-06	1.04E-04	1	PAH
1-Methoxypyrene	8.93E-02	8.44E-01	3.88E-01	4.06E-01	3.13E-02	1.95E-02	9.02E-04	2.56E-03	4.08E-05	8.92E-04	1	PAH
Atherosperminine	1.59E-01	2.11E-01	1.02E-01	2.17E-01	1.48E-02	2.14E-02	1.85E-02	8.14E-03	8.57E-03	3.04E-03	1	PAH
Indoxyl sulfate	1.00E-02	3.57E-03	5.22E-03	9.29E-03	1.33E-05	1.70E-03	8.21E-04	1.96E-07	1.62E-03	3.04E-04	1	Indole
Indole-3-acetic-acid-O-glucuronide	2.83E-02	9.52E-05	5.09E-08	2.41E-07	3.78E-03	1.69E-04	4.28E-02	2.30E-05	2.28E-02	1.53E-03	1	Indole
Tocopheronic acid	1.94E-01	3.71E-01	4.33E-01	2.84E-02	3.63E-02	2.15E-02	1.46E-02	3.61E-04	4.18E-05	4.61E-04	1	OBR
Piperoic acid	1.14E-01	1.20E-01	3.85E-03	5.38E-02	2.10E-02	1.66E-03	4.79E-03	3.66E-03	6.36E-03	4.61E-04	1	OBR
Dopamine	4.84E-04	1.78E-02	1.24E-07	3.92E-05	1.21E-08	8.31E-06	8.66E-09	2.28E-06	2.54E-06	8.92E-04	1	OBR
Aspidospermatine	1.23E-03	1.04E-03	1.45E-04	8.88E-05	2.20E-05	2.87E-05	5.34E-05	1.90E-05	3.46E-04	8.92E-04	1	OBR
Caffeic acid 3-O-glucuronide	2.97E-01	2.23E-02	2.51E-03	9.89E-03	3.05E-03	1.64E-03	1.03E-02	1.28E-03	1.01E-02	1.67E-03	1	OBR
Hydroxykynurenine	6.41E-01	4.24E-01	4.44E-03	1.44E-01	5.27E-03	3.28E-02	5.80E-03	6.67E-03	3.16E-03	1.67E-03	1	OBR
5-Hydroferulic acid	8.64E-05	1.30E-03	1.07E-04	1.51E-04	1.46E-05	5.17E-04	3.56E-03	2.05E-02	1.77E-02	3.04E-03	1	OBR
4-Aminohippuric acid	4.95E-02	1.92E-02	4.29E-02	4.42E-02	1.03E-02	1.23E-02	6.23E-03	9.30E-03	1.48E-03	3.04E-03	1	OBR
Glutaminylphenylalanine	6.92E-03	2.10E-02	9.86E-04	5.78E-04	1.94E-03	3.17E-04	7.08E-03	8.79E-05	1.13E-04	3.04E-03	1	OBR
N,N-Dimethylaniline	5.57E-03	5.19E-04	1.41E-04	2.43E-03	6.14E-05	2.00E-03	5.71E-04	2.74E-04	7.09E-04	5.37E-03	1	OBR
Phenylpropionylglycine	1.05E-01	1.91E-02	4.04E-02	8.40E-02	4.75E-04	1.86E-04	7.01E-03	3.15E-04	2.59E-04	5.37E-03	1	OBR
Phenethylamine glucuronide	2.62E-03	7.70E-04	5.97E-06	1.64E-05	3.99E-06	1.50E-05	4.42E-06	4.18E-06	6.37E-04	9.21E-03	1	OBR
Benzaldehyde	4.85E-03	7.36E-03	1.45E-02	2.63E-03	1.46E-02	1.48E-03	7.12E-03	1.36E-03	1.31E-03	2.48E-02	1	OBR
4-Hydroxybenzylamine	5.85E-05	4.32E-02	7.39E-03	2.24E-02	7.44E-04	9.87E-03	1.42E-02	1.49E-05	3.03E-05	3.89E-02	1	OBR

Abbreviations: OBR, one benzene ring; PAH, polycyclic aromatic hydrocarbon.

[a]*P* values were calculated from a one-way ANOVA.

[b]Trend *P* value was computed using original regression.

[c]Changed tendency of metabolites in chronic kidney disease (CKD) progression. 1 indicated increased metabolites in CKD progression; −1 indicated decreased metabolites in CKD progression.

expressions of aryl hydrocarbon receptor and its target genes were determined throughout the study period. As shown in Figure 3a, the mRNA expression of aryl hydrocarbon receptor was significantly up-regulated, which was accompanied by up-regulation of aryl hydrocarbon receptor target genes including *CYP1A1*, *CYP1A2* and *CYP1B1* (Figure 3a). Similarly, the significantly up-regulated aryl hydrocarbon receptor protein level in the nuclei was accompanied by significant down-regulation of the aryl hydrocarbon receptor protein level in the cytoplasm, suggesting the activation of aryl hydrocarbon receptor signalling (Figure 3b,c). Additionally, immuno-histochemical staining showed that nuclear translocation of aryl hydrocarbon receptor in tubular epithelial cells was observed at Weeks 2, 9 and 12 (Figure 3d). In addition, aryl hydrocarbon receptor expression in the nuclei was significantly up-regulated in patients with idiopathic membranous nephropathy, diabetic nephropathy and IgA nephropathy (Figure 3e). These findings demonstrated that aryl hydrocarbon receptor signalling could be activated by aryl-containing metabolite in chronic kidney disease patients. Collectively, these findings indicated that chronic kidney disease is associated with aryl hydrocarbon receptor activation.

3.5 | Activation of aryl hydrocarbon receptor signalling by aryl-containing metabolite during chronic kidney disease progression

Dock can automatically simulate the action of the ligand at the active site of the receptor and exhibit the mode of interaction. We next investigated whether aryl hydrocarbon receptor could be activated by aryl-containing metabolite based on molecular docking. The interactions between the ligand-binding domain of rat aryl hydrocarbon receptor and the six metabolites were studied. The result showed that all the six metabolites could bind to the ligand-binding site of aryl hydrocarbon receptor to different degrees (Figures 3f). In addition, indole-3-acetic-acid-O-glucuronide showed a lower Ki value than 2,3,7,8-tetrachlorodibenzo-p-dioxin and the other metabolites showed a similar Ki value to 2,3,7,8-tetrachlorodibenzo-p-dioxin (Table S7), suggesting that these metabolites had strong affinities with aryl hydrocarbon receptor. The interactions among the amino acids of rat aryl hydrocarbon receptor and the six metabolites are shown in Figure 3g. The hydroxyl group of 1-hydroxypyrene formed a hydrogen bond with Tyr308 and showed a pi–pi interaction with Phe322. 1-Methoxypyrene showed two pi–pi interactions with Phe285 and Phe322. Other interactions are presented in Figure 3h.

3.6 | Toxicity of 1-aminopyrene on NRK-52E cells

Based on the results of *P* value, the correlation coefficients between aryl-containing metabolite and serum creatinine or creatinine clearance rate and molecular docking, 1-aminopyrene was selected for the subsequent experiments. We further explored the toxicity of 1-aminopyrene on NRK-52E cell viability. As shown in Figure 4a, the cell viability was gradually reduced with increasing concentrations of 1-aminopyrene. Moreover, there was significant cell death when the 1-aminopyrene treatment lasted up to 48 h.

3.7 | 1-Aminopyrene activated the expression of aryl hydrocarbon receptor and its target genes

We next examined whether 1-aminopyrene could activate aryl hydrocarbon receptor in NRK-52E cells. The protein expression of nuclear aryl hydrocarbon receptor was significantly up-regulated upon treatment with 0.1, 1 and 10 nM of 1-aminopyrene for 24 h, while the cytoplasmic aryl hydrocarbon receptor expression was significantly down-regulated, highlighting the activation of aryl hydrocarbon receptor (Figure 4b,c). Similarly, aryl hydrocarbon receptor was activated upon treatment with 10 nM of 1-aminopyrene for 6, 12 and 24 h (Figure 4d,e). Luciferase assays showed that 1-aminopyrene significantly enhanced the aryl hydrocarbon receptor-driven reporter activity (Figure 4f). In addition, the mRNA expression of aryl hydrocarbon receptor was up-regulated by 1-aminopyrene stimulation for 24 h in a dose-independent manner (Figure 4g). We also investigated the effect of 1-aminopyrene on aryl hydrocarbon receptor expression in mice and discovered that the mRNA expressions of aryl hydrocarbon receptor and its target genes including *CYP1A1*, *CYP1A2* and *CYP1B1* were significantly up-regulated at Weeks 3, 6 and 9 (Figure 4h). Additionally, the nuclear aryl hydrocarbon receptor expression was significantly up-regulated and there was obvious nuclear translocation in mice treated with 1-aminopyrene in the third week, suggesting the activation of aryl hydrocarbon receptor (Figure 4i–l). We then depleted the aryl hydrocarbon receptor levels in NRK-52E cells by transfection of shRNA targeting aryl hydrocarbon receptor mRNA, which significantly down-regulated the aryl hydrocarbon receptor levels after 24 h (Figure 4m). Mass spectrometry imagining showed that the 1-aminopyrene levels were significantly increased in the kidney cortex and medulla of the mice (Figure 4n), indicating that 1-aminopyrene could reach the kidneys by oral administration. *CYP1A1*, *CYP1A2* and *CYP1B1* were significantly reduced in aryl hydrocarbon receptor shRNA-induced NRK-52E cells induced by 1-aminopyrene (Figure 4o). aryl hydrocarbon receptor shRNA led to a significant reduction in aryl hydrocarbon receptor mRNA expression (Figure 4p). Three target genes of aryl hydrocarbon receptor were significantly reduced in aryl hydrocarbon receptor shRNA-treated mice induced by 1-aminopyrene (Figure 4q). We further found that the levels of serum creatinine and urea significantly increased in 1-aminopyrene-induced mice compared to that in control mice (Figure 4r). 1-Aminopyrene treatment also led to renal injury and fibrosis in mice (Figure 4s,t). Collectively, these findings demonstrated that renal fibrosis was mediated partially through aryl
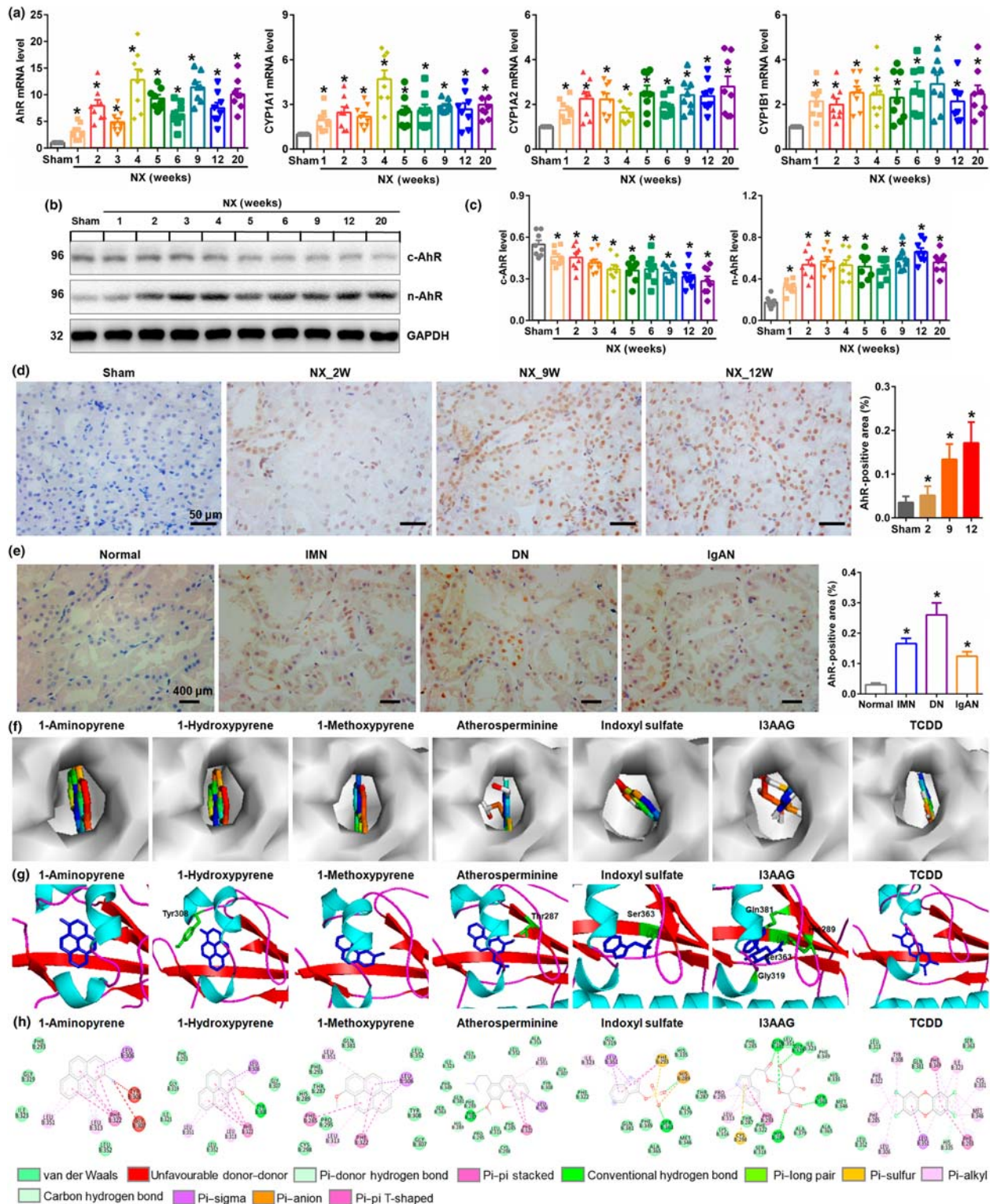
FIGURE 3 Aryl hydrocarbon receptor (AhR) signalling was activated by aryl-containing metabolite (ACM) in progressive chronic kidney disease (CKD). (a) The mRNA expression levels of AhR and its target genes including *CYP1A1*, *CYP1A2* and *CYP1B1* throughout the entire study period. (b) Protein expression of AhR in the nuclei and cytoplasm of the remnant kidney of the rats throughout the entire study period. (c) Quantitative analysis of AhR expression in the nuclei and cytoplasm of the remnant kidney of the rats. (d) Immunohistochemical findings with anti-AhR in the remnant kidney of the rats at Weeks 2, 9 and 12. (e) Immunohistochemical findings with anti-AhR in the kidney tissue of patients with idiopathic membranous nephropathy (IMN), diabetic nephropathy (DN) and IgA nephropathy (IgAN). (f) The binding sites of ACM in the Periodic Acid-Schiff (PAS)-B domain of rat AhR. (g, h) The interaction of ACM with the amino acids of rat AhR. Hydrogen bonds are shown in green and pi–sulfur interaction is shown in orange (g). The dot represents a single-data point in the bar graph. *$P < 0.05$ versus sham group ($n = 8$)
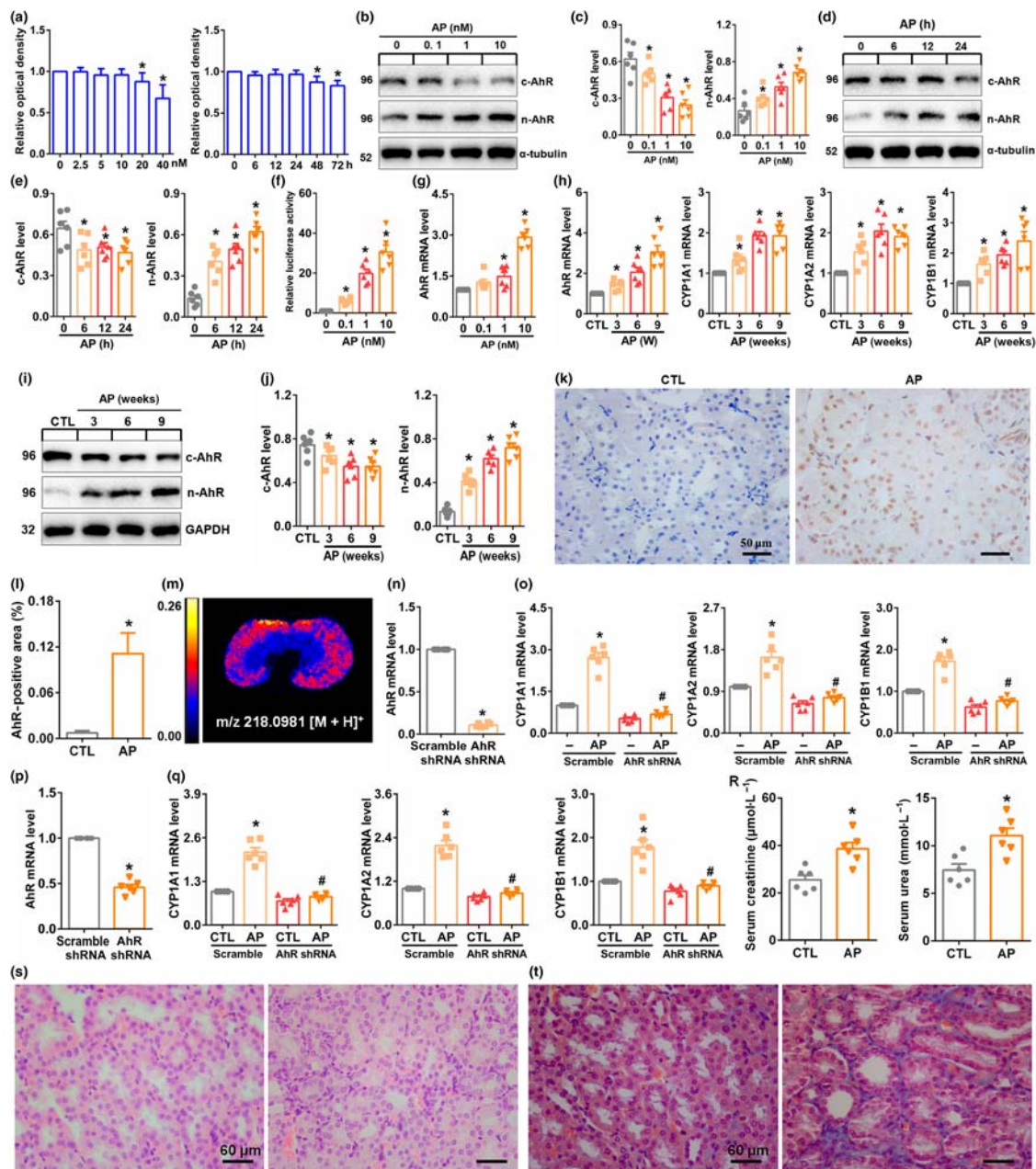
FIGURE 4 Aryl hydrocarbon receptor (AhR) signalling was activated by 1-aminopyrene (AP). (a) Cell viability after treatment with increasing concentrations of AP (0–40 μM) in NRK-52E cells for 24 h and cell viability after treatment with 10-nM AP at different time points. (b) Protein expression of AhR in the nuclei and cytoplasm of NRK-52E cells induced by AP at the different concentrations. (c) Quantitative analysis of the AhR expression of NRK-52E cells induced by AP at different concentrations. (d) Protein expression of AhR in the nuclei and cytoplasm of NRK-52E cells induced by AP at different time points. (e) Quantitative analysis of the AhR expression of NRK-52E cells induced by AP at different time points. (f) The mRNA expression levels of AhR in NRK-52E cells induced by AP at different concentrations. (g) Luciferase assays of AhR activation in NRK-52E cells induced by AP for 24 h at different concentrations. (h) The mRNA expression levels of AhR and its target genes including *CYP1A1*, *CYP1A2* and *CYP1B1* in mice induced by AP at Weeks 3, 6 and 9. (i) Protein expression of AhR in the nuclei and cytoplasm of mice induced by AP at Weeks 3, 6 and 9. (j) Quantitative analysis of the AhR expression of mice induced by AP at Weeks 3, 6 and 9. (k) Immunohistochemical findings with anti-AhR in mice induced by AP at Week 9. (l) Quantitative analysis of immunohistochemistry with anti-AhR in mice induced by AP. (m) mRNA expression of AhR studied by comparative qRT-PCR in NRK-52E transfected with scramble shRNA or AhR shRNA. (n) Representative MSI of AP in kidney tissues in mice induced by AP. (o) After transfection with AhR-specific shRNA or scrambled shRNA, the mRNA expression levels of AhR target genes including *CYP1A1*, *CYP1A2* and *CYP1B1* in AP-induced NRK-52E cells at 24 h. (p) AhR mRNA expression levels in AhR shRNA-treated mice at Week 9. (q) mRNA expression levels of AhR target genes including *CYP1A1*, *CYP1A2* and *CYP1B1* in AhR shRNA-treated mice induced by AP at Week 9. (r) The levels of serum creatinine and urea in control and AP-induced mice at Week 9. (s) Images for HE staining in control and AP-induced mice at Week 9. (t) Images for Masson's trichrome staining from control and AP-induced mice at Week 9. $*P < 0.05$ versus CTL group ($n = 6$). $\#P < 0.05$ versus scramble shRNA or AhR shRNA group ($n = 6$)

hydrocarbon receptor activation induced by 1-aminopyrene, indicating that aryl hydrocarbon receptor could have been activated by endogenous metabolites.

3.8 | The identification of natural flavonoids from Semen Plantaginis as aryl hydrocarbon receptor antagonists

We screened and identified a flavonoid aglycone 5,7,3′,4′,5′-pentahydroxy flavanone and two flavonoid glycosides including barleriside A and rhoifolin from Semen Plantaginis, in the basis of molecular docking and aryl hydrocarbon receptor mRNA expression in 1-aminopyrene-induced NRK-52E cells (Figure 5a). The results showed that all three flavonoids could bind to the active site of the Periodic Acid-Schiff-B domain of rat aryl hydrocarbon receptor and that they showed a strong interaction with rat aryl hydrocarbon receptor (Figures 5b and S1). The ΔG values of 5,7,3′,4′,5′-pentahydroxy flavanone, barleriside A, rhoifolin and CH223191 were −8.64, −8.32, −10.14 and −9.85, respectively. The Ki values of 5,7,3′,4′,5′-pentahydroxy flavanone, barleriside A, rhoifolin and CH223191 were 461.85, 798.99, 36.86 and 60.47 nM, respectively. Notably, BAS and rhoifolin showed stronger antagonistic effects on aryl hydrocarbon receptor activity compared to CH233191. Collectively, these findings indicated that the three flavonoids are potent aryl hydrocarbon receptor antagonists.

3.9 | Flavonoids attenuated renal injury via inhibiting aryl hydrocarbon receptor activation-mediated aryl-containing metabolite

We next determined whether the three flavonoids antagonized aryl hydrocarbon receptor activity in 1-aminopyrene-induced NRK-52E cells. Treatment with 1-aminopyrene led to a significant increase in aryl hydrocarbon receptor expression in the nuclei and treatment with the three flavonoids significantly decreased 1-aminopyrene-induced nuclear aryl hydrocarbon receptor expression in NRK-52E cells (Figure 5c), suggesting that the three flavonoids could inhibit aryl-containing metabolite-induced aryl hydrocarbon receptor activation (Figure 5d,e). The mRNA expression of aryl hydrocarbon receptor target genes was also inhibited by flavonoid treatment (Figure 5f). Furthermore, 1-aminopyrene significantly enhanced the aryl hydrocarbon receptor-driven reporter activity, which was inhibited by flavonoid treatment, indicating that the three flavonoids could directly target aryl hydrocarbon receptor activity (Figure 5g). We further showed that treatment with the three flavonoids abrogated the 1-aminopyrene-induced up-regulation of profibrotic protein expression in NRK-52E cells, indicating that renal fibrosis was attenuated by flavonoids (Figure 5h,i). Collectively, the results indicated that the flavonoids alleviated renal

fibrosis via inhibiting aryl-containing metabolite-induced aryl hydrocarbon receptor activation.

3.10 | Dietary flavonoids retarded chronic kidney disease via antagonizing aryl hydrocarbon receptor activation by mediation through aryl-containing metabolite

Both 5,7,3′,4′,5′-pentahydroxy flavanone and barleriside A treatments significantly alleviated the up-regulation of nuclear aryl hydrocarbon receptor and the down-regulation of cytoplasmic aryl hydrocarbon receptor expression (Figure 6a,b). Additionally, these treatments significantly down-regulated the mRNA expression of aryl hydrocarbon receptor target genes (Figure 6c). Meanwhile, their treatment significantly reduced the levels of six aryl-containing metabolites (Figure 6d). We further found that treatment with 5,7,3′,4′,5′-pentahydroxy flavanone and BSF significantly lowered the serum creatinine, urea and proteinuria levels in 5/6 nephrectomized rats, while the renal function was significantly improved (Figure 6e). As shown in Figure 6f, there were interstitial inflammation and renal fibrosis in the 5/6 nephrectomized rats, while treatment with 5,7,3′,4′,5′-pentahydroxy flavanone and BSF significantly down-regulated collagen I and α-smooth muscle actin expressions and further alleviated TIF. However, treatment with 5,7,3′,4′,5′-pentahydroxy flavanone and BSF produced a slightly inhibitory effect on glomerular injury (data not shown). Additionally, treatment with 5,7,3′,4′,5′-pentahydroxy flavanone and BSF inhibited the up-regulation of fibronectin, vimentin and fibroblast-specific protein 1 expressions and preserved E-cadherin expression (Figure 6g,h). Collectively, aryl-containing metabolite-induced aryl hydrocarbon receptor activation is involved in renal fibrosis and dietary flavonoids show a potential antifibrotic effect in 5/6 nephrectomized rats.

3.11 | Barleriside A mitigates epithelial-to-mesenchymal transition partly via targeting the antagonism of aryl hydrocarbon receptor activation

Finally, we determined whether flavonoids could directly antagonize aryl hydrocarbon receptor activation and mitigate renal fibrosis. Our results showed that barleriside A was the strongest aryl hydrocarbon receptor antagonist. Compared to scramble shRNA transfection, aryl hydrocarbon receptor shRNA transfection resulted in a significant decline in aryl hydrocarbon receptor protein expression in NRK-52E cells (Figure 7a). Barleriside A treatment did not produce a significant effect on aryl hydrocarbon receptor expression in aryl hydrocarbon receptor shRNA-treated HK-2 cells (Figure 7b). Barleriside A treatment showed a strong inhibitory effect on the mRNA expression of aryl hydrocarbon receptor target genes in 1-aminopyrene-induced NRK-52E cells after aryl hydrocarbon receptor overexpression (Figure 7c). Similarly, barleriside A treatment was observed for the antifibrotic effect of barleriside A (Figure 7d,e). Collectively, these
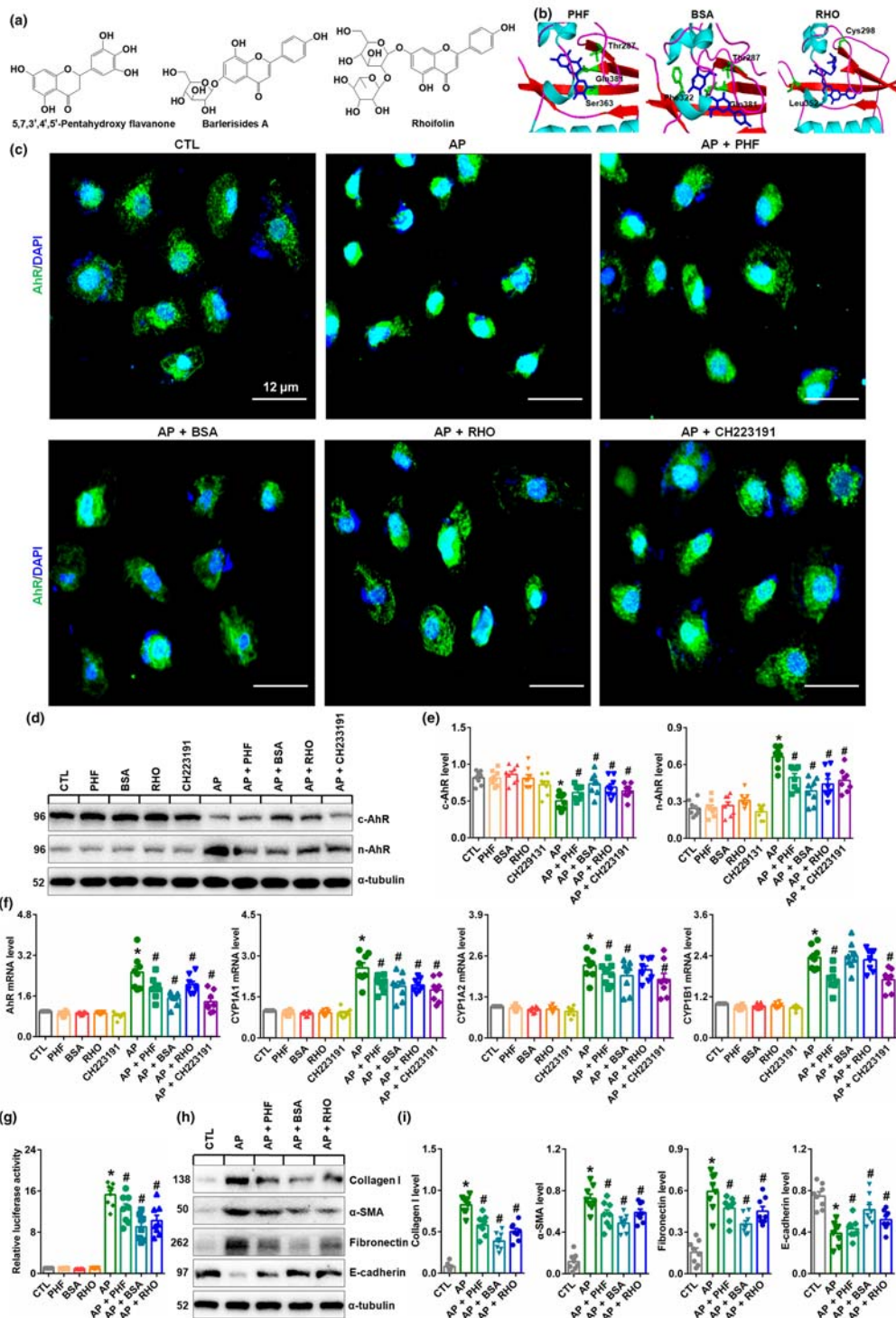
FIGURE 5 Flavonoids mitigate epithelial-to-mesenchymal transition (EMT) through blocking aryl hydrocarbon receptor (AhR) in 1-aminopyrene (AP)-induced NRK-52E cells. (a) Chemical structure of three flavonoids including 5,7,3′,4′,5′-pentahydroxy flavanone (PHF), barleriside A (BSA) and rhoifolin (RHO). (b) The interaction of PHF, BSA and RHO with the amino acids of rat AhR. (c) Representative immunofluorescent staining indicating AP-induced AhR expression in AP-induced NRK-52E cells upon treatment with flavonoids or CH223191. (d) Protein expression of AhR in nuclei and cytoplasm in the different groups. (e) Quantitative analysis of AhR in nuclei and cytoplasm from the different groups, as indicated. (f) The mRNA expression levels of AhR target genes including *CYP1A1*, *CYP1A2* and *CYP1B1* from the different groups, as indicated. (g) Luciferase assays of AhR activation from the different groups, as indicated. (h) Protein expression of collagen I, α-smooth muscle actin(α-SMA), fibronectin and E-cadherin in the different groups, as indicated. (i) Quantitative analysis of collagen I, α-SMA, fibronectin and E-cadherin in the different groups, as indicated. The dot represents a single-data point in the bar graph. $^{*}P < 0.05$ versus CTL group ($n = 6$). $^{\#}P < 0.05$ versus AP-induced group ($n = 6$)
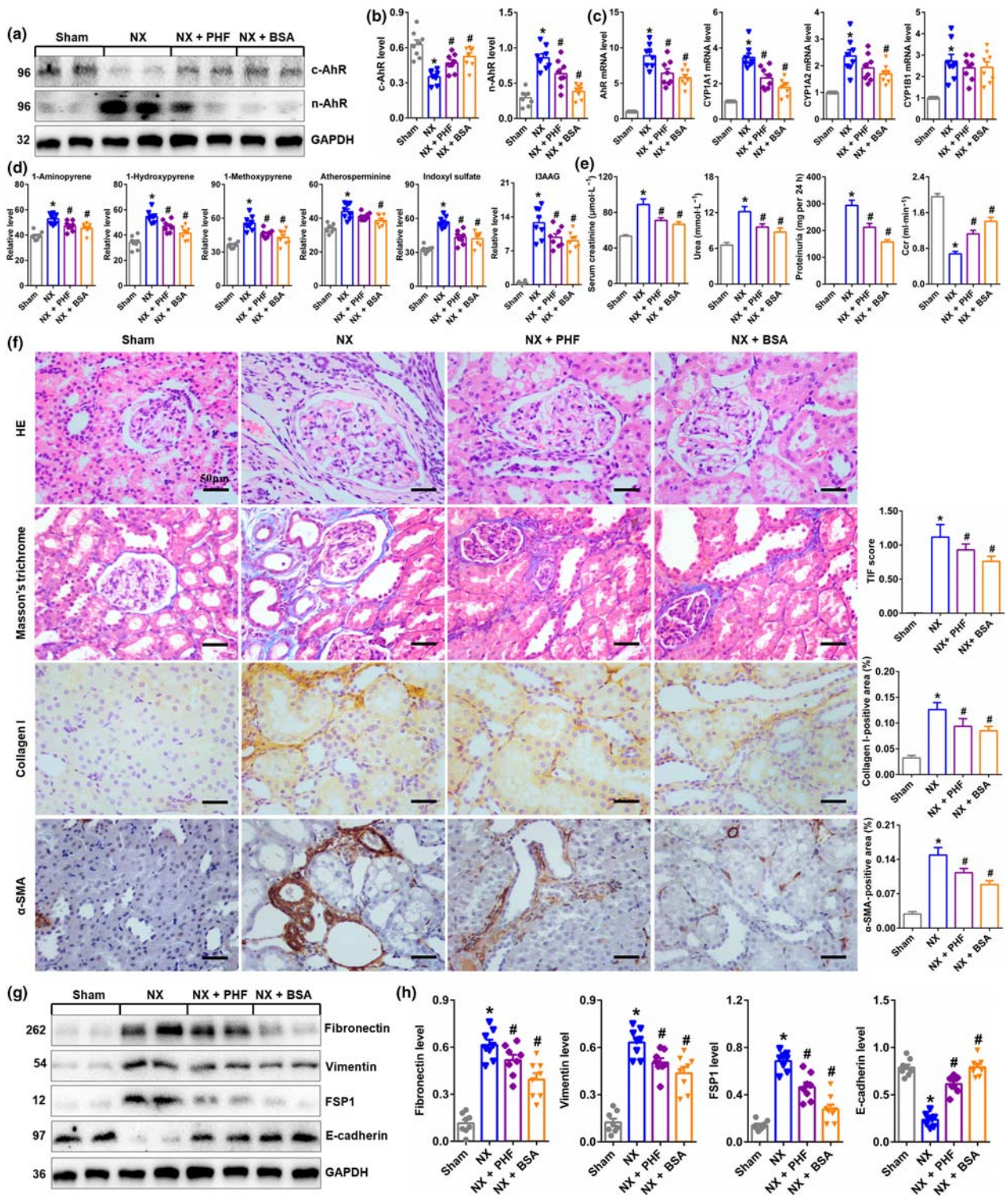
FIGURE 6 Dietary flavonoids retarded chronic kidney disease (CKD) and renal fibrosis via antagonizing aryl hydrocarbon receptor (AhR) activation mediated by aryl-containing metabolite ACM in 5/6 nephrectomized (NX) rats. (a) Protein expression of AhR in nuclei and cytoplasm from the different rats, as indicated, at Week 12. (b) Quantitative analysis of AhR expression in nuclei and cytoplasm from the different rats, as indicated, at Week 12. (c) The mRNA expression levels of AhR target genes including *CYP1A1*, *CYP1A2* and *CYP1B1* from the different rats, as indicated, at Week 12. (d) The intensity of six ACMs from the different rats, as indicated, at Week 12. (e) Clinical biochemistry from the different rats, as indicated, at Week 12. (f) Images of HE staining, Masson's trichrome staining and immunohistochemical staining of collagen I and α-SMA expressions from different rats, as indicated, at Week 12. (g) Protein expressions of fibronectin, vimentin, fibroblast-specific protein 1 (FSP1) and E-cadherin from different rats, as indicated, at Week 12. (h) Quantitative analysis of fibronectin, vimentin, FSP1 and E-cadherin from different rats, as indicated, at Week 12. The dot represents a single-data point in the bar graph. *$P < 0.05$ versus sham group ($n = 6$); #$P < 0.05$ versus NX group ($n = 6$)
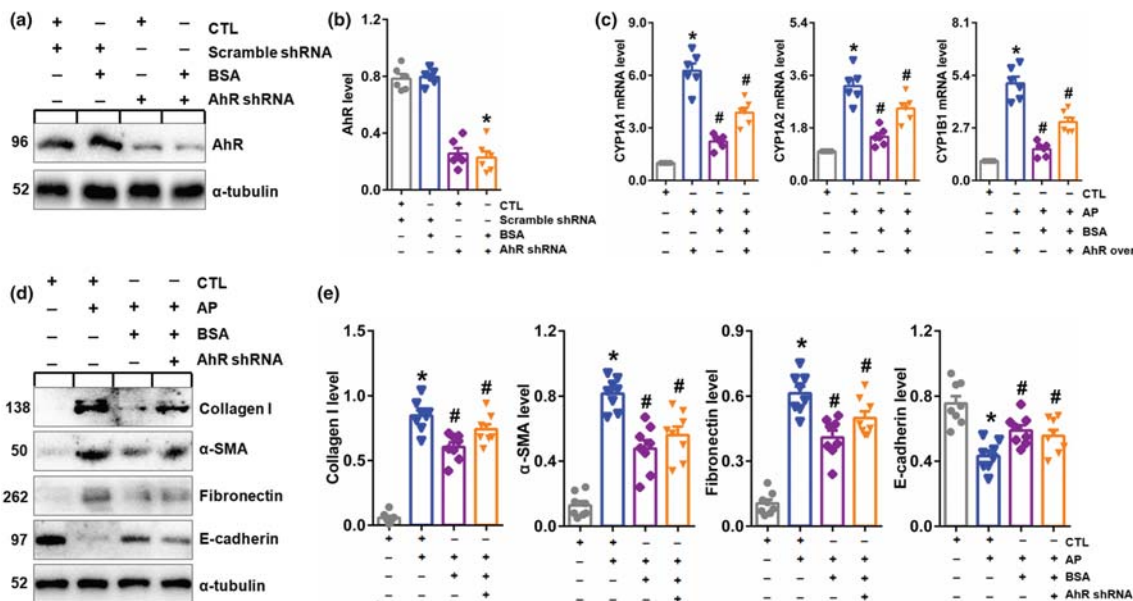
FIGURE 7 Barleriside A (BSA) mitigated epithelial-to-mesenchymal transition (EMT) via partly targeting the antagonism of aryl hydrocarbon receptor (AhR) activation. (a) The protein expression of AhR in NRK-52E cells induced by AhR shRNA. (b) Quantitative analysis of AhR expression in NRK-52E cells induced by AhR shRNA. (c) mRNA expression levels of AhR target genes including *CYP1A1*, *CYP1A2* and *CYP1B1* in 1-aminopyrene (AP)-induced NRK-52E cells treated with BSA after AhR overexpression. (d) Protein expression of collagen I, α-SMA, fibronectin and E-cadherin in AP-induced NRK-52E cells treated with BSA after transfection with AhR-specific shRNA or scrambled shRNA. (e) Quantitative analyses of protein expression of collagen I, α-SMA, fibronectin and E-cadherin in AP-induced NRK-52E cells treated with BSA. *$P < 0.05$ versus CTL group ($n = 6$); #$P < 0.05$ versus AP group ($n = 6$)

findings indicated that the antifibrotic effect of barleriside A might be associated with activation of aryl hydrocarbon receptor signalling pathway.

4 | DISCUSSION

Using the least absolute shrinkage and selection operator procedure, we demonstrated that six aryl-containing metabolites were significantly increased in a rodent model of chronic kidney disease. In line with this result, our study also demonstrated that six aryl-containing metabolites were significantly increased in patients with idiopathic membranous nephropathy, diabetic nephropathy and IgA nephropathy (Figure 8). Our current study demonstrated significant up-regulation of aryl hydrocarbon receptor protein level in nuclei and mRNA accompanied by up-regulation of aryl hydrocarbon receptor target genes in 5/6 nephrectomized rats, indicating that 5/6 nephrectomy leads to aryl hydrocarbon receptor activation (Figure 8). Because polycyclic aromatic hydrocarbons are the classical ligands of aryl hydrocarbon receptor, we speculated that aryl hydrocarbon receptor activation might be associated with the dysregulation of endogenous metabolites. Molecular docking showed that six aryl-containing metabolites including 1-aminopyrene had strong affinities. Our study further demonstrated that 1-aminopyrene could mediate aryl hydrocarbon receptor expression in both mice and NRK-52E cells (Figure 8). Furthermore, 1-aminopyrene treatment significantly up-regulated the mRNA expressions of aryl hydrocarbon receptor and its three target

genes, which were partially attenuated in aryl hydrocarbon receptor shRNA-treated NRK-52E cells and mice (Figure 8). Collectively, these findings demonstrated that aryl hydrocarbon receptor could be activated by aryl-containing metabolite. In addition, two flavonoids including 5,7,3′,4′,5′-pentahydroxy flavanone and barleriside A could antagonize aryl hydrocarbon receptor activity in both 1-aminopyrene-induced NRK-52E cells and 5/6 nephrectomized rats (Figure 8). Barleriside A mitigates epithelial-to-mesenchymal transition (EMT) partly via targeting and antagonizing aryl hydrocarbon receptor activation (Figure 8). Collectively, our results demonstrated that flavonoids could mitigate epithelial-to-mesenchymal transition by selectively inhibiting aryl hydrocarbon receptor activation.

We identified six aryl-containing metabolites that had the most prominent effects on renal injury. 1-Aminopyrene is a metabolite of 1-nitropyrene. Our MSI showed that the 1-aminopyrene levels were significantly increased in the kidney cortex and medulla of 1-aminopyrene-induced mice. It was reported that 1-aminopyrene induced *CYP1B1* expression in the kidney tissue of rats (Hatanaka et al., 2001). 1-Aminopyrene also induced *CYP1B1* expression in in vitro experiments (Iwanari, Nakajima, Kizu, Hayakawa, & Yokoi, 2002). In addition, 1-aminopyrene could lead to extensive oxidative damage and promote the expression of proinflammatory cytokines (Wu, Jiang, Liu, Shang, & An, 2018). We first identified that high AP levels in kidney tissues contributed to renal injury through activation of aryl hydrocarbon receptor and its target genes. These data support the activation of aryl hydrocarbon receptor by aryl-containing metabolite during the progression of chronic kidney disease.
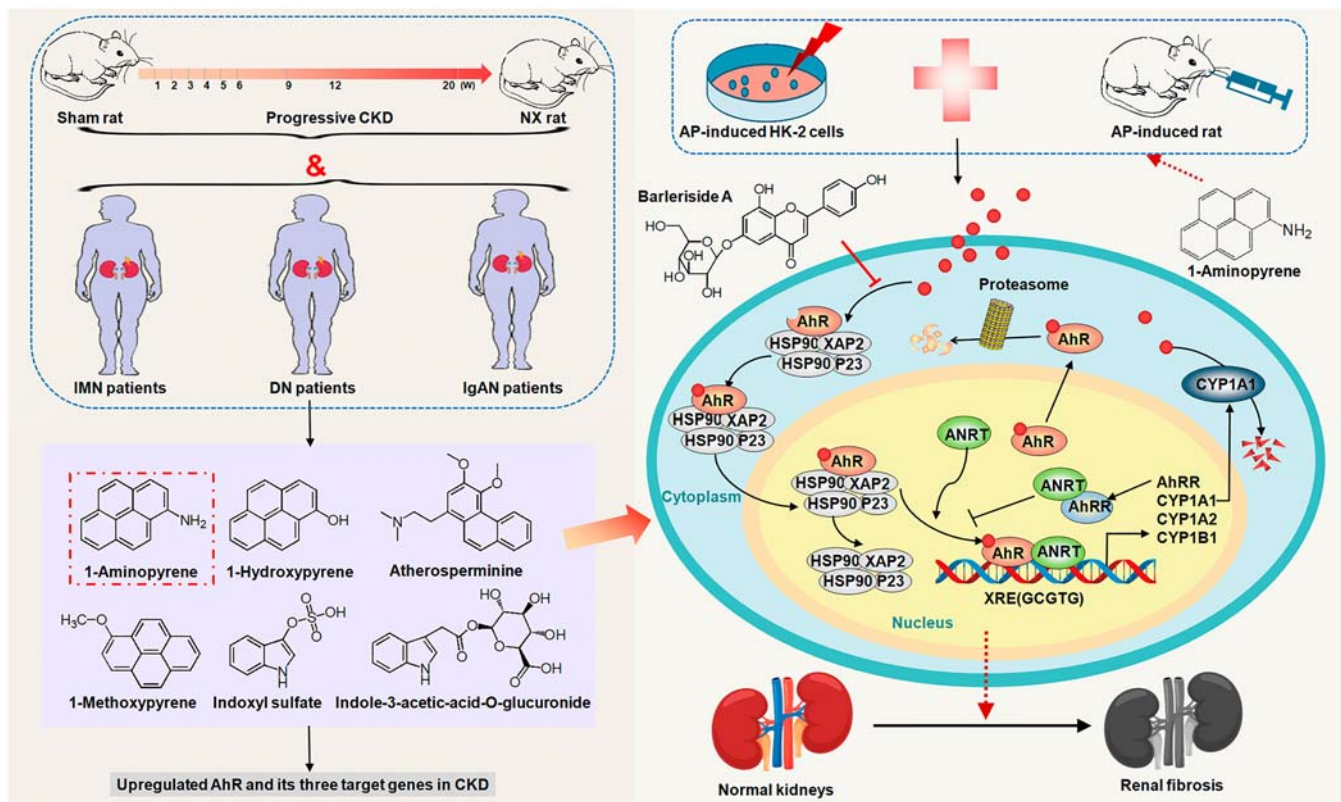
FIGURE 8 Summary of molecular mechanism of aryl hydrocarbon receptor (AhR) activation by ACM in progressive chronic kidney disease (CKD). AhR signalling and its target genes were activated in both 5/6 nephrectomized (NX) rats and patients with idiopathic membranous nephropathy (IMN), diabetic nephropathy (DN) and IgA nephropathy (IgAN). Flavonoids ameliorated CKD and renal fibrosis through inhibiting AhR activity via lowering the increased levels of six ACMs

Our current study identified several uraemic toxins including tryptophan-derived metabolites such as indoxyl sulfate, hippuric acid, kynurenine and hydroxykynurenine in 5/6 nephrectomized rats. Tryptophan-derived uraemic toxins could activate aryl hydrocarbon receptor signalling through direct binding with aryl hydrocarbon receptor, inducing its nuclear translocation and activation of transcription of its target genes in the cultured cells (Gondouin et al., 2013; Schroeder et al., 2010). Extensive evidence has demonstrated that both animals and patients with chronic kidney disease have high indoxyl sulfate level in both serum and kidney tissues (Dou et al., 2018). Increased aryl hydrocarbon receptor-activating potential of the serum from chronic kidney disease patients strongly correlated with eGFR and indoxyl sulfate levels and the CYP1A1 expression was up-regulated in the whole blood from chronic kidney disease patients (Dou et al., 2018). Further study showed that increased aryl hydrocarbon receptor-activating potential of serum and CYP1A1 mRNA were demonstrated in the aorta and heart of 5/6 nephrectomized mice. Serial indoxyl sulfate injections led to increased aryl hydrocarbon receptor-activating potential of serum and CYP1A1 mRNA expression in the aorta and heart in wild-type mice but not in *aryl hydrocarbon receptor*$^{-/-}$ mice (Dou et al., 2018). Our previous findings revealed that indoxyl sulfate induced a fivefold and sevenfold increase in serum of unilateral ureteral obstruction rats and kidney tissues of rats with chronic renal failure (Chen, Chen, et al., 2019; Zhao et al., 2014; Zhao,

Cheng, et al., 2013; Zhao, Lei, Chen, Feng, & Bai, 2013). In addition, another study has shown a significantly increased CYP1A2 protein expression in the renal tissue of chronic kidney disease rats (Sindhu & Vaziri, 2003). Conversely, it has been demonstrated that indole-induced aryl hydrocarbon receptor activation contributed to mucosal homeostasis. *Lactobacillus* spp. could regulate IL-22 mucosal homeostasis through indolealdehyde-mediated aryl hydrocarbon receptor activation and protect mice against mucosal candidiasis (Zelante et al., 2013). Another study showed that the treatment of mice with three *Lactobacillus* strains could metabolize tryptophan and alleviate intestinal inflammation through aryl hydrocarbon receptor activation, as the effects were abolished by an aryl hydrocarbon receptor antagonist (Lamas et al., 2016). In addition, *aryl hydrocarbon receptor*$^{-/-}$ mice showed earlier spatial memory impairment and enhanced astrogliosis in the hippocampus when compared to age-matched *aryl hydrocarbon receptor*$^{+/+}$ controls, suggesting a link between aryl hydrocarbon receptor and aging (Bravo-Ferrer et al., 2019). Collectively, the current work and that of others suggested that aryl hydrocarbon receptor could be activated by aryl-containing metabolite during chronic kidney disease progression.

In our recent reviews, we summarized that a myriad of natural products have been reported to exhibit beneficial effects against renal fibrosis (Chen, Hu, et al., 2018; Chen, Yang, et al., 2018; Chen, Yu, et al., 2019; Chen, Feng, Cao, & Zhao, 2018; Feng, Chen, Vaziri,

Guo, & Zhao, 2019). Flavonoids are the most abundant polyphenols contained in the diet and over 15,000 flavonoids have been separated and identified from various plants (Xiao, 2017). Emerging evidence has demonstrated that flavonoids are the largest category of aryl hydrocarbon receptor ligands (Yang, Feng, Chen, Vaziri, & Zhao, 2019). Treatment of three flavonoids including 5,7,3′,4′,5′-pentahydroxy flavanone, barleriside A and rhoifolin abrogated the up-regulation of fibrotic protein expression in 1-aminopyrene-exposed NRK-52E cells. Similarly, treatment with both 5,7,3′,4′,5′-pentahydroxy flavanone and barleriside A ameliorated chronic kidney disease and renal fibrosis through inhibiting the aryl hydrocarbon receptor activity via lowering the increased level of six aryl-containing metabolites in 5/6 nephrectomized rats.

In summary, six aryl-containing metabolites were significantly increased in both 5/6 nephrectomized rats and patients with chronic kidney disease and they were associated with the activation of aryl hydrocarbon receptor and its target genes throughout the study period. aryl hydrocarbon receptor could be activated by aryl-containing metabolite during chronic kidney disease progression and dietary flavonoids retard renal fibrosis by inhibiting aryl hydrocarbon receptor activity via lowering the aryl-containing metabolite levels. 1-Aminopyrene could significantly up-regulate the mRNA expression of aryl hydrocarbon receptor and its target genes including *CYP1A1*, *CYP1A2* and *CYP1B1* in both mice and NRK-52E cells. Mass spectrometry imagining showed that 1-aminopyrene levels were significantly increased in the kidney cortex and medulla of mice. Therefore, aryl hydrocarbon receptor might be an antifibrotic target, the inhibition of which may be a promising strategy to confer antifibrotic benefit in patients with chronic kidney disease.

ACKNOWLEDGEMENTS

AUTHOR CONTRIBUTIONS

Y.-Y.Z. conceived and designed the experiments. H.M., G.C., X.-Q.W., Y.-Y.C., D.-Q.C., L.C. and Y.-L.F. conducted and analysed the experiments. Y.G. and Y.-Y.Z. performed statistical analysis. W.S., Y.G., X.-Y.Y. and L.Z. collected the clinical samples. H.M. and Y.-Y.Z. wrote the initial draft of the manuscript. S.Z. and N.D.V. revised the manuscript. All authors have critically revised the manuscript and approved its final version.

CONFLICT OF INTEREST

The authors declare no conflict of interest.

DECLARATION OF TRANSPARENCY AND SCIENTIFIC RIGOUR

This declaration acknowledges that this paper adheres to the principles for transparent reporting and scientific rigour of preclinical research as stated in the *BJP* guidelines for Design & Analysis, Immunoblotting and Immunochemistry and Animal Experimentation and as recommended by funding agencies, publishers and other organizations engaged with supporting research.

ORCID

Shougang Zhuang https://orcid.org/0000-0001-9719-4187
Ying-Yong Zhao https://orcid.org/0000-0002-0239-7342

REFERENCES

Alexander, S. P. H., Fabbro, D., Kelly, E., Mathie, A., Peters, J. A., Veale, E. L., … CGTP Collaorators. (2019). The Concise Guide to PHARMACOLOGY 2019/20: Enzymes. *British Journal of Pharmacology*, *176*(Suppl 1), S297–s396.

Alexander, S. P. H., Kelly, E., Mathie, A., Peters, J. A., Veale, E. L., Armstrong, J. F., … Wong, S. S. (2019). The Concise Guide To PHARMACOLOGY 2019/20: Introduction and other protein targets. *British Journal of Pharmacology*, *176*(Suppl 1), S1–s20.

Alexander, S. P. H., Roberts, R. E., Broughton, B. R. S., Sobey, C. G., George, C. H., Stanford, S. C., … Ahluwalia, A. (2018). Goals and practicalities of immunoblotting and immunohistochemistry: A guide for submission to the British Journal of Pharmacology. *British Journal of Pharmacology*, *175*, 407–411. https://doi.org/10.1111/bph.14112

Bisson, W. H., Koch, D. C., O'Donnell, E. F., Khalil, S. M., Kerkvliet, N. I., Tanguay, R. L., … Kolluri, S. K. (2009). Modeling of the aryl hydrocarbon receptor (AhR) ligand binding domain and its utility in virtual ligand screening to predict new AhR ligands. *Journal of Medicinal Chemistry*, *52*, 5635–5641. https://doi.org/10.1021/jm900199u

Bravo-Ferrer, I., Cuartero, M. I., Medina, V., Ahedo-Quero, D., Pena-Martinez, C., Perez-Ruiz, A., … Moro, M. A. (2019). Lack of the aryl hydrocarbon receptor accelerates aging in mice. *The FASEB Journal*, *33*, 12644–12654. https://doi.org/10.1096/fj.201901333R

Brito, J. S., Borges, N. A., Esgalhado, M., Magliano, D. C., Soulage, C. O., & Mafra, D. (2017). Aryl hydrocarbon receptor activation in chronic kidney disease: Role of uremic toxins. *Nephron*, *137*, 1–7. https://doi.org/10.1159/000476074

Chen, D. Q., Cao, G., Chen, H., Argyopoulos, C. P., Yu, H., Su, W., … Zhao, Y. Y. (2019). Identification of serum metabolites associating with chronic kidney disease progression and anti-fibrotic effect of 5-methoxytryptophan. *Nature Communications*, *10*, 1476. https://doi.org/10.1038/s41467-019-09329-0

Chen, D. Q., Feng, Y. L., Cao, G., & Zhao, Y. Y. (2018). Natural products as a source for antifibrosis therapy. *Trends in Pharmacological Sciences*, *39*, 937–952. https://doi.org/10.1016/j.tips.2018.09.002

Chen, D. Q., Hu, H. H., Wang, Y. N., Feng, Y. L., Cao, G., & Zhao, Y. Y. (2018). Natural products for the prevention and treatment of kidney disease. *Phytomedicine*, *50*, 50–60. https://doi.org/10.1016/j.phymed.2018.09.182

Chen, L., Chen, D. Q., Liu, J. R., Zhang, J., Vaziri, N. D., Zhuang, S., … Zhao, Y.-Y. (2019). Unilateral ureteral obstruction causes gut microbial dysbiosis and metabolome disorders contributing to tubulointerstitial fibrosis. *Experimental & Molecular Medicine*, *51*, 1–18.

Chen, L., Yang, T., Lu, D. W., Zhao, H., Feng, Y. L., Chen, H., … Zhao, Y. Y. (2018). Central role of dysregulation of TGF-β/Smad in CKD progression and potential targets of its treatment. *Biomedicine & Pharmacotherapy*, *101*, 670–681. https://doi.org/10.1016/j.biopha.2018.02.090

Chen, Y. Y., Yu, X. Y., Chen, L., Vaziri, N. D., Ma, S. C., & Zhao, Y. Y. (2019). Redox signaling in aging kidney and opportunity for therapeutic intervention through natural products. *Free Radical Biology & Medicine*, *141*, 141–149. https://doi.org/10.1016/j.freeradbiomed.2019.06.012

Cheong, J. E., & Sun, L. (2018). Targeting the IDO1/TDO2-KYN-AhR pathway for cancer immunotherapy—Challenges and opportunities. *Trends*

in Pharmacological Sciences, 39, 307–325. https://doi.org/10.1016/j.tips.2017.11.007

Choi, H. Y., Lim, J. E., & Hong, J. H. (2010). Curcumin interrupts the interaction between the androgen receptor and Wnt/β-catenin signaling pathway in LNCaP prostate cancer cells. *Prostate Cancer and Prostatic Diseases*, 13, 343–349. https://doi.org/10.1038/pcan.2010.26

Chung, W., Chen, J., Turman, C., Lindstrom, S., Zhu, Z., Loh, P. R., ... Liang, L. (2019). Efficient cross-trait penalized regression increases prediction accuracy in large cohorts using secondary phenotypes. *Nature Communications*, 10, 569. https://doi.org/10.1038/s41467-019-08535-0

Corre, S., Tardif, N., Mouchet, N., Leclair, H. M., Boussemart, L., Gautron, A., ... Galibert, M. D. (2018). Sustained activation of the Aryl hydrocarbon Receptor transcription factor promotes resistance to BRAF-inhibitors in melanoma. *Nature Communications*, 9, 4775. https://doi.org/10.1038/s41467-018-06951-2

Curtis, M. J., Alexander, S., Cirino, G., Docherty, J. R., George, C. H., Giembycz, M. A., ... Ahluwalia, A. (2018). Experimental design and analysis and their reporting II: Updated and simplified guidance for authors and peer reviewers. *British Journal of Pharmacology*, 175, 987–993. https://doi.org/10.1111/bph.14153

Dolivo, D. M., Larson, S. A., & Dominko, T. (2018). Tryptophan metabolites kynurenine and serotonin regulate fibroblast activation and fibrosis. *Cellular and Molecular Life Sciences*, 75, 3663–3681. https://doi.org/10.1007/s00018-018-2880-2

Dolkart, O., Khoury, W., Amar, E., & Weinbroum, A. A. (2014). Pneumoperitoneum in the presence of acute and chronic kidney injury: An experimental model in rats. *The Journal of Urology*, 192, 1266–1271. https://doi.org/10.1016/j.juro.2014.03.114

Dou, L., Poitevin, S., Sallee, M., Addi, T., Gondouin, B., McKay, N., ... Burtey, S. (2018). Aryl hydrocarbon receptor is activated in patients and mice with chronic kidney disease. *Kidney International*, 93, 986–999. https://doi.org/10.1016/j.kint.2017.11.010

Dou, L., Sallee, M., Cerini, C., Poitevin, S., Gondouin, B., Jourde-Chiche, N., ... Burtey, S. (2015). The cardiovascular effect of the uremic solute indole-3 acetic acid. *American Society of Nephrology*, 26, 876–887. https://doi.org/10.1681/ASN.2013121283

Feng, Y. L., Cao, G., Chen, D. Q., Vaziri, N. D., Chen, L., Zhang, J., ... Zhao, Y.-Y. (2019). Microbiome-metabolomics reveals gut microbiota associated with glycine-conjugated metabolites and polyamine metabolism in chronic kidney disease. *Cellular and Molecular Life Sciences*, 74, 4961–4978.

Feng, Y. L., Chen, D. Q., Vaziri, N. D., Guo, Y., & Zhao, Y. Y. (2019). Small molecule inhibitors of epithelial-mesenchymal transition for the treatment of cancer and fibrosis. *Medicinal Research Reviews*, 40, 54–78.

Gansevoort, R. T., Correa-Rotter, R., Hemmelgarn, B. R., Jafar, T. H., Heerspink, H. J., Mann, J. F., ... Wen, C. P. (2013). Chronic kidney disease and cardiovascular risk: Epidemiology, mechanisms, and prevention. *Lancet*, 382, 339–352. https://doi.org/10.1016/S0140-6736(13)60595-4

Ginalski, K. (2006). Comparative modeling for protein structure prediction. *Current Opinion in Structural Biology*, 16, 172–177. https://doi.org/10.1016/j.sbi.2006.02.003

Gondouin, B., Cerini, C., Dou, L., Sallee, M., Duval-Sabatier, A., Pletinck, A., ... Burtey, S. (2013). Indolic uremic solutes increase tissue factor production in endothelial cells by the aryl hydrocarbon receptor pathway. *Kidney International*, 84, 733–744. https://doi.org/10.1038/ki.2013.133

Gutierrez-Vazquez, C., & Quintana, F. J. (2018). Regulation of the immune response by the aryl hydrocarbon receptor. *Immunity*, 48, 19–33. https://doi.org/10.1016/j.immuni.2017.12.012

Hao, S., Bellner, L., & Ferreri, N. R. (2013). NKCC2A and NFAT5 regulate renal TNF production induced by hypertonic NaCl intake. *American Journal of Physiology. Renal Physiology*, 304, F533–F542. https://doi.org/10.1152/ajprenal.00243.2012

Harding, S. D., Sharman, J. L., Faccenda, E., Southan, C., Pawson, A. J., Ireland, S., ... NC-IUPHAR. (2018). The IUPHAR/BPS Guide to PHARMACOLOGY in 2018: Updates and expansion to encompass the new guide to IMMUNOPHARMACOLOGY. *Nucleic Acids Research*, 46, D1091–d1106. https://doi.org/10.1093/nar/gkx1121

Hatanaka, N., Yamazaki, H., Kizu, R., Hayakawa, K., Aoki, Y., Iwanari, M., ... Yokoi, T. (2001). Induction of cytochrome P450 1B1 in lung, liver and kidney of rats exposed to diesel exhaust. *Carcinogenesis*, 22, 2033–2038. https://doi.org/10.1093/carcin/22.12.2033

Iu, M., Zago, M., Rico de Souza, A., Bouttier, M., Pareek, S., White, J. H., ... Baglole, C. J. (2017). RelB attenuates cigarette smoke extract-induced apoptosis in association with transcriptional regulation of the aryl hydrocarbon receptor. *Free Radical Biology & Medicine*, 108, 19–31. https://doi.org/10.1016/j.freeradbiomed.2017.02.045

Iwanari, M., Nakajima, M., Kizu, R., Hayakawa, K., & Yokoi, T. (2002). Induction of CYP1A1, CYP1A2, and CYP1B1 mRNAs by nitropolycyclic aromatic hydrocarbons in various human tissue-derived cells: Chemical-, cytochrome P450 isoform-, and cell-specific differences. *Archives of Toxicology*, 76, 287–298. https://doi.org/10.1007/s00204-002-0340-z

Iyoda, M., Shibata, T., Hirai, Y., Kuno, Y., & Akizawa, T. (2011). Nilotinib attenuates renal injury and prolongs survival in chronic kidney disease. *J Am Soc Nephrol*, 22, 1486–1496. https://doi.org/10.1681/ASN.2010111158

Kilkenny, C., Browne, W., Cuthill, I. C., Emerson, M., & Altman, D. G. (2010). Animal research: Reporting in vivo experiments: The ARRIVE guidelines. *British Journal of Pharmacology*, 160, 1577–1579. https://doi.org/10.1111/j.1476-5381.2010.00872.x

Kim, M., Chen, S. W., Park, S. W., Kim, M., D'Agati, V. D., Yang, J., & Lee, H. T. (2009). Kidney-specific reconstitution of the A1 adenosine receptor in A1 adenosine receptor knockout mice reduces renal ischemia-reperfusion injury. *Kidney International*, 75, 809–823. https://doi.org/10.1038/ki.2008.699

Lamas, B., Richard, M. L., Leducq, V., Pham, H. P., Michel, M. L., Da Costa, G., ... Sokol, H. (2016). CARD9 impacts colitis by altering gut microbiota metabolism of tryptophan into aryl hydrocarbon receptor ligands. *Nature Medicine*, 22, 598–605. https://doi.org/10.1038/nm.4102

Li, H., Liu, J., Chen, J., Wang, H., Yang, L., Chen, F., ... Song, E. (2018). A serum microRNA signature predicts trastuzumab benefit in HER2-positive metastatic breast cancer patients. *Nature Communications*, 9, 1614. https://doi.org/10.1038/s41467-018-03537-w

Lin, S. L., Chen, Y. M., Chien, C. T., Chiang, W. C., Tsai, C. C., & Tsai, T. J. (2002). Pentoxifylline attenuated the renal disease progression in rats with remnant kidney. *American Society of Nephrology*, 13, 2916–2929. https://doi.org/10.1097/01.asn.0000034909.10994.8a

Ma, D., Xie, H. Q., Zhang, W., Xue, Q., Liu, X., Xu, L., ... Zhao, B. (2019). Aryl hydrocarbon receptor activity of polyhalogenated carbazoles and the molecular mechanism. *Science of the Total Environment*, 687, 516–526. https://doi.org/10.1016/j.scitotenv.2019.05.406

Rodriguez-Iturbe, B., Ferrebuz, A., Vanegas, V., Quiroz, Y., Espinoza, F., Pons, H., & Vaziri, N. D. (2005). Early treatment with cGMP phosphodiesterase inhibitor ameliorates progression of renal damage. *Kidney International*, 68, 2131–2142. https://doi.org/10.1111/j.1523-1755.2005.00669.x

Sallee, M., Dou, L., Cerini, C., Poitevin, S., Brunet, P., & Burtey, S. (2014). The aryl hydrocarbon receptor-activating effect of uremic toxins from tryptophan metabolism: A new concept to understand cardiovascular complications of chronic kidney disease. *Toxins*, 6, 934–949. https://doi.org/10.3390/toxins6030934

Schroeder, J. C., Dinatale, B. C., Murray, I. A., Flaveny, C. A., Liu, Q., Laurenzana, E. M., ... Perdew, G. H. (2010). The uremic toxin 3-indoxyl sulfate is a potent endogenous agonist for the human aryl hydrocarbon receptor. *Biochemistry*, 49, 393–400. https://doi.org/10.1021/bi901786x

Shinde, R., & McGaha, T. L. (2018). The aryl hydrocarbon receptor: Connecting immunity to the microenvironment. *Trends in Immunology*, *39*, 1005–1020. https://doi.org/10.1016/j.it.2018.10.010

Shivanna, S., Kolandaivelu, K., Shashar, M., Belghasim, M., Al-Rabadi, L., Balcells, M., … Chitalia, V. C. (2016). The aryl hydrocarbon receptor is a critical regulator of tissue factor stability and an antithrombotic target in uremia. *Journal of the American Society of Nephrology*, *27*, 189–201. https://doi.org/10.1681/ASN.2014121241

Sindhu, R. K., & Vaziri, N. D. (2003). Upregulation of cytochrome P450 1A2 in chronic renal failure: Does oxidized tryptophan play a role? *Advances in Experimental Medicine and Biology*, *527*, 401–407. https://doi.org/10.1007/978-1-4615-0135-0_47

Song, P., Ramprasath, T., Wang, H., & Zou, M. H. (2017). Abnormal kynurenine pathway of tryptophan catabolism in cardiovascular diseases. *Cellular and Molecular Life Sciences*, *74*, 2899–2916. https://doi.org/10.1007/s00018-017-2504-2

Wang, J., Xie, P., Huang, J. M., Qu, Y., Zhang, F., Wei, L. G., … Huang, X. J. (2016). The new Asian modified CKD-EPI equation leads to more accurate GFR estimation in Chinese patients with CKD. *International Urology and Nephrology*, *48*, 2077–2081. https://doi.org/10.1007/s11255-016-1386-9

Wang, M., Chen, D. Q., Chen, L., Cao, G., Zhao, H., Liu, D., … Zhao, Y. Y. (2018). Novel inhibitors of the cellular renin-angiotensin system components, poricoic acids, target Smad3 phosphorylation and Wnt/β-catenin pathway against renal fibrosis. *British Journal of Pharmacology*, *175*, 2689–2708. https://doi.org/10.1111/bph.14333

Wu, M., Jiang, Y., Liu, M., Shang, Y., & An, J. (2018). Amino-PAHs activated Nrf2/ARE anti-oxidative defense system and promoted inflammatory responses: The regulation of PI3K/Akt pathway. *Toxicology Research (Camb)*, *7*, 465–472. https://doi.org/10.1039/c8tx00010g

Xiao, J. (2017). Dietary flavonoid aglycones and their glycosides: Which show better biological significance? *Critical Reviews in Food Science and Nutrition*, *57*, 1874–1905. https://doi.org/10.1080/10408398.2015.1032400

Yang, T., Feng, Y. L., Chen, L., Vaziri, N. D., & Zhao, Y. Y. (2019). Dietary natural flavonoids treating cancer by targeting aryl hydrocarbon receptor. *Critical Reviews in Toxicology*, *49*, 445–460. https://doi.org/10.1080/10408444.2019.1635987

Zelante, T., Iannitti, R. G., Cunha, C., De Luca, A., Giovannini, G., Pieraccini, G., … Romani, L. (2013). Tryptophan catabolites from microbiota engage aryl hydrocarbon receptor and balance mucosal reactivity via interleukin-22. *Immunity*, *39*, 372–385. https://doi.org/10.1016/j.immuni.2013.08.003

Zhang, S., Li, S., Zhou, Z., Fu, H., Xu, L., Xie, H. Q., & Zhao, B. (2018). Development and application of a novel bioassay system for dioxin determination and aryl hydrocarbon receptor activation evaluation in ambient-air samples. *Environmental Science & Technology*, *52*, 2926–2933. https://doi.org/10.1021/acs.est.7b06376

Zhang, Z. H., Vaziri, N. D., Wei, F., Cheng, X. L., Bai, X., & Zhao, Y. Y. (2016). An integrated lipidomics and metabolomics reveal nephroprotective effect and biochemical mechanism of Rheum officinale in chronic renal failure. *Scientific Reports*, *6*, 22151. https://doi.org/10.1038/srep22151

Zhang, Z. H., Wei, F., Vaziri, N. D., Cheng, X. L., Bai, X., Lin, R. C., & Zhao, Y. Y. (2015). Metabolomics insights into chronic kidney disease and modulatory effect of rhubarb against tubulointerstitial fibrosis. *Scientific Reports*, *5*, 14472. https://doi.org/10.1038/srep14472

Zhao, H., Chen, L., Yang, T., Feng, Y. L., Vaziri, N. D., Liu, B. L., … Zhao, Y. Y. (2019). Aryl hydrocarbon receptor activation mediates kidney disease and renal cell carcinoma. *Journal of Translational Medicine*, *17*, 302. https://doi.org/10.1186/s12967-019-2054-5

Zhao, Y. Y., Chen, H., Tian, T., Chen, D. Q., Bai, X., & Wei, F. (2014). A pharmaco-metabonomic study on chronic kidney disease and therapeutic effect of ergone by UPLC-QTOF/HDMS. *PLoS ONE*, *23*, e115467.

Zhao, Y. Y., Cheng, X. L., Cui, J. H., Yan, X. R., Wei, F., Bai, X., & Lin, R. C. (2012). Effect of ergosta-4,6,8(14),22-tetraen-3-one (ergone) on adenine-induced chronic renal failure rat: A serum metabonomic study based on ultra performance liquid chromatography/high-sensitivity mass spectrometry coupled with MassLynx i-FIT algorithm. *Clinica Chimica Acta*, *413*, 1438–1445. https://doi.org/10.1016/j.cca.2012.06.005

Zhao, Y. Y., Cheng, X. L., Wei, F., Bai, X., Tan, X. J., Lin, R. C., & Mei, Q. (2013). Intrarenal metabolomic investigation of chronic kidney disease and its TGF-β1 mechanism in induced-adenine rats using UPLC Q-TOF/HSMS/MS^E. *Journal of Proteome Research*, *12*, 2692–2703.

Zhao, Y. Y., Cheng, X. L., Wei, F., Xiao, X. Y., Sun, W. J., Zhang, Y., & Lin, R. C. (2012). Serum metabonomics study of adenine-induced chronic renal failure in rats by ultra performance liquid chromatography coupled with quadrupole time-of-flight mass spectrometry. *Biomarkers*, *17*, 48–55. https://doi.org/10.3109/1354750X.2011.637180

Zhao, Y. Y., Lei, P., Chen, D. Q., Feng, Y. L., & Bai, X. (2013). Renal metabolic profiling of early renal injury and renoprotective effects of *Poria cocos* epidermis using UPLC Q-TOF/HSMS/MS^E. *Journal of Pharmaceutical and Biomedical Analysis*, *81-82*, 202–209. https://doi.org/10.1016/j.jpba.2013.03.028

Zhao, Y. Y., Liu, J., Cheng, X. L., Bai, X., & Lin, R. C. (2012). Urinary metabonomics study on biochemical changes in an experimental model of chronic renal failure by adenine based on UPLC Q-TOF/MS. *Clinica Chimica Acta*, *413*, 642–649.

Zhao, Y. Y., Zhang, L., Long, F. Y., Cheng, X. L., Bai, X., Wei, F., & Lin, R. C. (2013). UPLC-Q-TOF/HSMS/MS^E-based metabonomics for adenine-induced changes in metabolic profiles of rat faeces and intervention effects of ergosta-4,6,8(14),22-tetraen-3-one. *Chemico-Biological Interactions*, *201*, 31–38. https://doi.org/10.1016/j.cbi.2012.12.002

SUPPORTING INFORMATION

Additional supporting information may be found online in the Supporting Information section at the end of this article.